Inorganic Chemistry

pubs.acs.org/IC Article

Planarity-Driven Structure–Morphology Correlations in a Co(II) Benzoylacetonate: Comparative Insights across the [M(bzac)$_2$] Family

Oumaima Ghodbane, Radhwane Takouachet, Rim Benali-Cherif,* Wahiba Falek, Alessia Bacchi, Andrea Daolio, El-Eulmi Bendeif, and Nourredine Benali-Cherif

Cite This: *Inorg. Chem.* 2026, 65, 3084–3101 Read Online

ACCESS | Metrics & More | Article Recommendations | Supporting Information

ABSTRACT: Advancing structure–packing–morphology correlations in β-diketonate complexes provides a rigorous framework for how local coordination geometry propagates into supramolecular organization and ultimately governs macroscopic form. Within this context, we report the synthesis, single-crystal and powder X-ray diffraction analysis, targeted CSD mining, BFDH morphology modeling, and complementary quantum calculations of a new cobalt(II) benzoylacetonate, [Co(bzac)$_2$]. Accurate SC-XRD data at 100 K establish a centrosymmetric trans-CoO$_4$ chromophore in $P2_1/n$ with a quasi square-planar coordination environment, while PXRD confirms phase purity. In the solid state, [Co(bzac)$_2$] forms directionally coherent zigzag stacks consistent with its experimentally observed acicular habit. A comparative CSD-survey across [M(bzac)$_2$] (M= Pb, Sn, Pdtrans, Pdcis, Cu) reveals metal-dependent variations in stereochemistry, chelate planarity, and packing, positioning the cobalt complex at the most planar and structurally coherent limit. BFDH analysis uncovers a monotonic increase in growth anisotropy culminating in [Co(bzac)$_2$], whose short π–π, metal–π, and C–H···π contacts rationalize its needle-like morphology. FTIR confirms enolization and O,O′-chelation, while UV–vis spectra display ligand-centered $\pi \rightarrow \pi^*$ and $n \rightarrow \pi^*$ transitions. DFT reproduces the experimental symmetry and electronic partitioning, and TD-DFT recovers the absorption envelope. Overall, the integrated SC-XRD ↔ CSD ↔ BFDH ↔ DFT workflow establishes [Co(bzac)$_2$] as a crystallographic, morphological, and electronic benchmark within the family.

1. INTRODUCTION

Coordination compounds based on O-donor ligands occupy a central place in contemporary inorganic and materials chemistry.[1−3] Beyond their classical roles in catalysis and homogeneous synthesis, such complexes underpin technologies in sensing, bioinorganic imaging, molecular electronics, and optoelectronics.[4−6] Their performance is governed by a hierarchy—primary coordination geometry around the metal, the extent of π-conjugation across the ligand framework,[7] and the resulting supramolecular packing in the solid state—each level modulating orbital overlap, charge delocalization, and energy transfer pathways at the molecular and mesoscale.[8] Understanding how these hierarchical factors cooperate is therefore critical for rational design strategies in anisotropic functional materials.

Among O-donor frameworks, β-diketonates are paradigmatic. Their chelating O,O′ bite fixes robust six-membered rings, confers predictable stereochemistry across diverse metals, and enables fine electronic tuning via substituents.[9] This combination makes β-diketonates ideal for dissecting how coordination symmetry propagates to intermolecular directionality and ultimately to crystal habit, with direct implications for thin-film emitters and related materials.[10−12]

Within this family, benzoylacetonate (bzac) provides an especially informative scaffold: the phenyl-substituted π-system enhances conjugation, the enolate/carbonyl couple enforces strong M–O interactions, and the rigid backbone promotes near-planarity of the chelate rings.[13] Because the O,O′ motif is conserved across metals, [M(bzac)$_2$] complexes form a controlled "chemical series" for isolating the influence of the metal's electronic configuration—from stereochemically active s^2 lone pairs in p-block cations[14,15] to ligand-field stabilization in d-block centers—on both local geometry and long-range assembly.[16] Despite the extensive crystallographic literature on metal β-diketonates, structure–property correlations within this family remain largely qualitative and fragmented. Previous studies have predominantly focused on individual metal centers or narrowly defined subsets of complexes, emphasizing local coordination geometry, electronic structure, or specific supramolecular motifs, often in the context of isolated crystal structures rather than systematically comparable series.[17−20] As a result, transferable descriptors that quantitatively relate coordination symmetry and chelate planarity to long-range packing organization and macroscopic crystal habit remain

Received: November 29, 2025
Revised: January 13, 2026
Accepted: January 16, 2026
Published: January 24, 2026

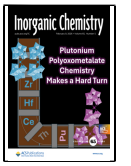

https://doi.org/10.1021/acs.inorgchem.5c05597
Inorg. Chem. 2026, 65, 3084−3101

Scheme 1. Synthetic Route to the $[Co(bzac)_2]$ Complex

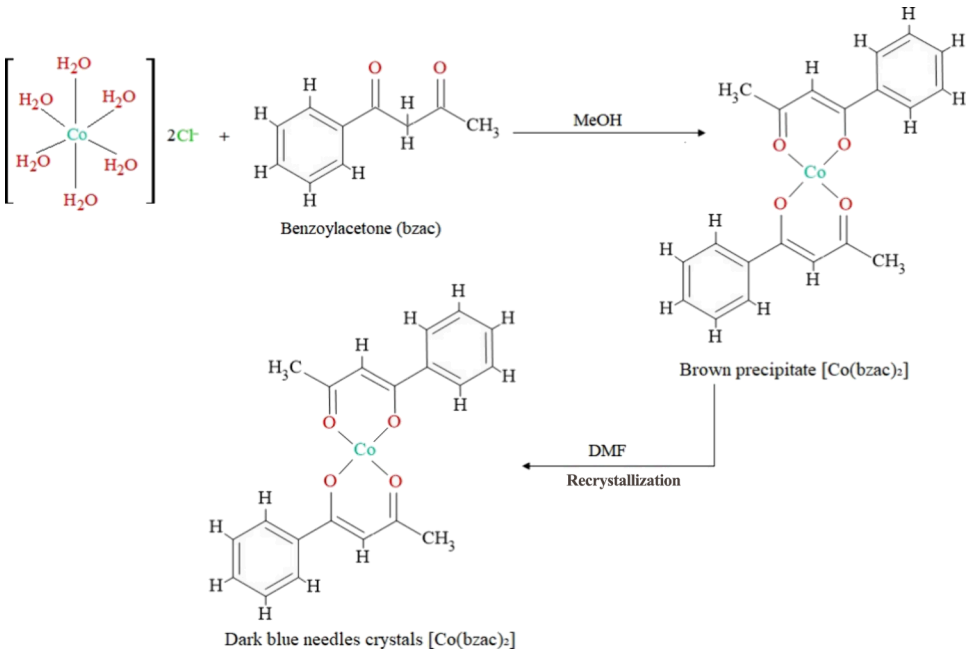

insufficiently defined across chemically coherent β-diketonate families. In particular, the extent to which subtle, metal-dependent variations in O,O′-chelate planarity propagate from the local coordination environment to anisotropic packing and morphology remains insufficiently quantified. Accordingly, metal β-diketonate complexes are still rarely exploited as benchmark systems for rationalizing crystal morphology from first-principles structural metrics.

Solid-state function depends not only on coordination at the molecular node but also on how molecules pack. Weak interactions—$\pi\cdots\pi$ overlaps between phenyl rings,[21] C−H$\cdots\pi$ contacts, and n(O)$\rightarrow\pi$ approaches—govern layering, slippage, and stacking metrics, thereby channeling exciton migration, modulating optical anisotropy, and biasing crystal growth along specific directions.[22,23] Capturing such links benefits from coupling single-crystal X-ray diffraction (SC-XRD) with morphology prediction (e.g., BFDH)[24] and electronic-structure analysis (DFT, FMOs, MEP/RDG).[25] Such integrative methodologies are especially effective for structurally constrained systems, where small geometric perturbations can be directly correlated with anisotropic packing and macroscopic growth behavior.

Within this context, a rigorously planar, centrosymmetric four-coordinate cobalt(II) β-diketonate represents a particularly powerful reference point. Unlike p-block congeners affected by stereochemically active lone pairs or d-block analogues exhibiting cis−trans variability or axial lability, a square-planar CoO_4 core enforced by inversion symmetry offers a structurally constrained and electronically well-defined platform. Such a system enables the isolation of planarity as a primary variable, disentangled from coordination number changes or ligand substitution effects, thereby allowing a direct assessment of how molecular flatness governs supramolecular cohesion, packing anisotropy, and crystal growth. This combination of enforced planarity, centrosymmetry, and electronic simplicity positions $[Co(bzac)_2]$ as an ideal reference against which deviations observed in other $[M(bzac)_2]$ analogues can be meaningfully assessed

This study reports the synthesis and experimental characterization of a new cobalt(II) benzoylacetonate, $[Co(bzac)_2]$, and situates it within a comparative framework spanning representative $[M(bzac)_2]$ analogues (Pb, Sn, Pdtrans, Pdcis, Cu) drawn from the Cambridge Structural Database. We combine SC-XRD and vibrational/UV−Vis spectroscopy with DFT (frontier orbitals, electrostatic maps) and BFDH morphology prediction to examine how metal-dependent stereochemistry and ligand π-delocalization relate to molecular planarity, packing organization, and crystal habit. By explicitly contrasting a structurally constrained reference system with less planar or stereochemically flexible congeners, the present approach overcomes limitations inherent to prior single-metal or case-specific β-diketonate studies. Our objective is to provide concise, method-anchored insights into planarity-driven structure−morphology correlations across the $[M(bzac)_2]$ family, while clarifying the structural and electronic significance of Co(II) within this comparative framework. Within this chemically and crystallographically coherent $[M(bzac)_2]$ series, $[Co(bzac)_2]$ is established as a benchmark compound for quantitatively correlating coordination planarity, noncovalent interaction topology, and crystal morphology, rather than serving as an isolated structural report. More broadly, the integrative approach developed here may serve as a model for designing coordination materials in which planarity, supramolecular cohesion, and packing anisotropy govern optical and morphological performance.

2. EXPERIMENTAL METHODS

2.1. Synthesis and Crystallization

All starting materials were purchased from Sigma-Aldrich and used without any further purification: cobalt(II) chloride hexahydrate ($CoCl_2\cdot 6H_2O$, 99.99%), 1-phenyl-1,3-butanedione (bzac, 99%), methanol (MeOH, ≥ 99%), and ethanol (EtOH, ≥ 99%). The $[Co(bzac)_2]$ complex was synthesized under ambient conditions. Cobalt(II) chloride hexahydrate (1 mmol, 0.238 g) was dissolved in 10 mL of methanol with continuous stirring. In a separate vessel, 1-phenyl-1,3-butanedione (0.324 g, 2 mmol) was dissolved in 15 mL of methanol. The ligand solution was then added dropwise to the cobalt

https://doi.org/10.1021/acs.inorgchem.5c05597
Inorg. Chem. 2026, 65, 3084−3101

solution under constant stirring at room temperature. The reaction mixture was stirred for 1 h, during which a brown precipitate gradually formed. The solid product was collected by filtration, washed several times with cold methanol, and air-dried. The obtained powder was recrystallized from dimethylformamide (DMF) by slow solvent evaporation at room temperature. After several weeks, dark blue needle-shaped crystals suitable for X-ray diffraction were obtained in 45% yield (Scheme 1).

2.2. Single Crystal X-ray Diffraction and Structure Refinement Details

Crystal data, experimental parameters, and structure refinement details for the title compound are listed in Table 1. Dark-blue needle-like single crystals, selected from the bulk material, were mounted on a MiTiGen loop coated with perfluoroether oil and measured on a Bruker D8 Venture diffractometer equipped with a PHOTON III CPAD detector. Data were collected at a constant temperature of T = 100 (2) K using Mo Kα radiation (λ = 0.71073 Å) in ω-scan mode. The structure was solved by direct methods using SHELXS[26] and refined by full-matrix least-squares on F^2 with SHELXL.[27] All non-hydrogen atoms were refined anisotropically, and hydrogen atoms were placed geometrically and refined using a riding model. A multiscan absorption correction was applied using SADABS 2016/2,[28] yielding an absorption coefficient of μ = 1.043 mm^{-1}, with T_{min} = 0.8610 and T_{max} = 1.0000. The refinement converged smoothly to R_1 = 0.0362 and wR_2 = 0.1103 for all reflections, with a goodness-of-fit on F^2 of 1.128. The final difference Fourier map revealed residual electron densities of +1.081 and − 0.677 e Å^{-3}, confirming an accurate model without significant disorder. All graphical representations were performed with Mercury 2025.3.[29]

Table 1. Main Crystallographic Data and Structure Refinement Details for Complex $[Co(bzac)_2]$

crystal data	
empirical formula	$C_{20}H_{18}CoO_4$
molecular weight (g/mol)	381.27
diffractometer	Bruker D8 Venture
radiation type	Mo Kα (λ = 0.71073 Å)
T (K)	100(2)
calculated density (Mg/m^3)	1.508
crystal system	monoclinic
space group	$P2_1/n$
a (Å)	4.3920 (17)
b (Å)	10.3955 (6)
c (Å)	18.497 (2)
β (°)	96.233 (16)
V (Å^3)	839.5 (3)
Z	2
μ (mm^{-1})	1.044
crystal size (mm)	0.20 × 0.08 × 0.07
T_{min}, T_{max}	0.861,1.000
no. of measured, independent and observed [$I > 2\sigma(I)$] reflections	82378, 4080, 3787
$R_{(int)}$[a]	0.051
refinement	
$R[F^2 > 2\sigma(F^2)]$[b], $wR(F^2)$[c], S[d]	0.034, 0.113, 1.13
no. of parameters	115
$\Delta\rho_{max}$, $\Delta\rho_{min}$ (e Å^{-3})	0.75, −0.65

[a] $R(int) = \Sigma(Fo^2 - < Fo^2>)] / \Sigma(Fo^2)$. [b] $R_1 = \Sigma||Fo|-|Fc|| / \Sigma|Fo|$. [c] $wR_2 = \{[\Sigma w(Fo^2-Fc^2)^2] / [\Sigma w(Fo^2)^2]\}^{1/2}$. [d] Goodness-of-fit $S = [\Sigma w(Fo^2 - Fc^2)^2/(n - p)]^{1/2}$, where n is the number of reflections and p the number of parameters.

2.3. Powder X-ray Diffraction (PXRD)

Powder X-ray diffraction measurements were performed at 296 K on a Rigaku SmartLab Multipurpose diffractometer equipped with Cu Kα radiation (λ = 0.154056 nm), operated at 40 kV and 30 mA. Data were collected in reflection geometry over the 2θ range 5−50° with a step size of 0.02°.

A simulated PXRD pattern was generated from the refined single-crystal structure (CCDC 2498791) using Mercury version 2025.3[29] to enable a direct structural comparison between the bulk microcrystalline sample and the SC-XRD model.

2.4. FTIR Analyses

Approximately 2 mg of complexe was scraped and subsequently compressed with 100 mg of dried spectroscopic grade KBr in a cold isostatic press at approximately 100 KPa. The FTIR spectra were acquired in transmission mode over the range of 400−4000 cm^{-1} at a resolution of 4 cm^{-1}, utilizing 64 scans on a PerkinElmer FT-IR spectrometer.

2.5. UV−Vis Analyses

Using a Spectroscan 80D UV−vis spectrophotometer, the $[Co(bzac)_2]$ absorption spectra were captured in DMF within the 190−500 nm wavelength range. The spectrophotometer was operated at a scan speed of 100 nm/min and a bandwidth of 2.0 nm.

2.6. Computational Details

Geometry optimization of $[Co(bzac)_2]$ was performed with DFT (B3LYP/LanL2DZ)[30] starting from the SC-XRD structure (CIF → MOL). Gas-phase optimizations were carried out without symmetry constraints in Gaussian 09W;[31] models were prepared/visualized in GaussView 6.0.[32] The calculations provided the optimized ground-state geometry, molecular electrostatic potential (MEP), frontier molecular orbital (HOMO/SOMO/LUMO) energies, Mulliken charges and Reduced density gradient (RDG)

3. RESULTS AND DISCUSSION

3.1. Crystal Structure and Supramolecular Features

The complex $[Co(bzac)_2]$ crystallizes in the monoclinic system, space group $P2_1/n$. The excellent refinement indicators confirm the high quality of the experimental data. The absence of significant residual electron density ($\Delta\rho_{max}$ = 0.75 e Å^{-3}; $\Delta\rho_{min}$ = − 0.65 e Å^{-3}) confirms the accuracy of the refined model and the structural integrity of the complex. The asymmetric unit consists of one-half of a cobalt(II) ion, located on an inversion center at (0, 1/2, 1/2), and one *bzac* ligand coordinated in a bidentate chelating mode through two oxygen atoms (O1 and O2) of the enolate and carbonyl groups. Each Co(II) atom is therefore surrounded by four oxygen donors—two from each of two symmetry-related *bzac* ligands—forming a distorted CoO_4 coordination sphere that completes a strictly square-planar geometry through inversion symmetry (Figure 1).

The Co−O bond distances are nearly identical [Co1−O1 = 1.9178(9) Å and Co1−O2 = 1.9209(8) Å], and the O−Co−O bond angles vary from 86.52(4)° to 93.48(4)°, consistent with a slightly distorted square-planar arrangement elongated along the trans O1−Co−O1 axis. The short and comparable Co−O distances reflect the strong donor ability of the enolate and carbonyl oxygens, typical of β-diketonate complexes.[33] Such geometries have been widely observed in *[Co(β-diketonate)$_2$]* systems, where electronic delocalization within the O−C−C−C−O fragment stabilizes the metal center and promotes planarity of the chelate rings.[34] The coordinated *bzac* ligand exhibits an almost planar conformation, with the Co atom lying close to the least-squares plane defined by O1−C1−C2−C3−O2. The aromatic phenyl substituent is nearly coplanar with the chelate ring (dihedral angle ≈ 12.15°), allowing for effective π-conjugation across the ligand backbone. This coplanarity supports partial delocalization of electron density from the enolate group to the aromatic π-system, a feature known to

https://doi.org/10.1021/acs.inorgchem.5c05597
Inorg. Chem. 2026, 65, 3084−3101

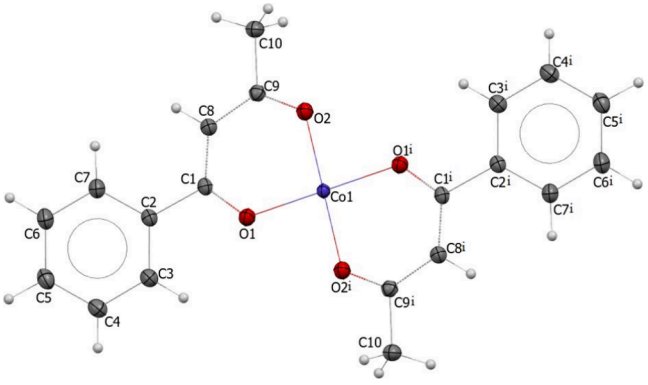

Figure 1. Perspective view of the $[Co(bzac)_2]$ complex with atom-labeling scheme. Displacement ellipsoids are drawn at the 50% probability level. Hydrogen atoms are shown as small spheres of arbitrary radius. Atoms labeled with the symbol "i" are generated by the crystallographic inversion center (symmetry code: (i) − x, − y, − z.)

influence the photophysical behavior of Co−β-diketone complexes.[35]

The crystal packing of $[Co(bzac)_2]$, reveals that the complexes are arranged in zigzag layers parallel to the *(b,c)* plane. Each molecule, lying on an inversion center, adopts an alternating orientation along the *b*-axis, producing a corrugated stacking pattern characteristic of the monoclinic space group $P2_1/n$. The nearly planar $[Co(bzac)_2]$ units are uniformly distributed within the unit cell, generating a well-organized three-dimensional framework with zigzag molecular alignment (Figure 2a). Interestingly, a similar zigzag packing mode has been reported for the tin(II) analogue, $[Sn(bzac)_2]$, by Paul F. R. Ewings et al.,[36] where the molecules also adopt an alternating arrangement along the monoclinic axes.

In the crystal packing, individual $[Co(bzac)_2]$ molecules are discrete rather than polymeric, but they are interconnected through a network of weak C−H···C, and $\pi-\pi$ stacking interactions. The $\pi-\pi$ contacts occur between adjacent phenyl rings with a centroid−centroid separation of ≈ 4.4 Å (Figure 2b), which lies in the expected range for aromatic stacking interactions in Co(II)−β-diketonates (3.8−4.4 Å).[37] These combined supramolecular forces ensure lattice stability and may facilitate intermolecular $\pi-\pi$ coupling, contributing to enhanced electronic communication across the crystal lattice.[38] These $\pi-\pi$ contacts play a dual structural and electronic role: they reinforce lattice cohesion and promote through-space $\pi-\pi$ coupling, enabling weak intermolecular charge delocalization and exciton migration. This mechanism has been correlated with enhanced optical responses and low-dimensional conductivity in Co−β-diketonate frameworks.[39,40]

Moderate C−H···C interactions constitute the main supramolecular linkages between neighboring $[Co(bzac)_2]$ units, reinforcing the cohesion of the crystal lattice. These contacts, involving aromatic hydrogen atoms approaching the π-clouds of adjacent phenyl rings, generate an extended three-dimensional framework stabilized by π-type interactions.[41] The molecular association results in the formation of well-defined graph-set motifs $R_4^4(36)$ and $R_4^4(30)$[42] (Figure 3a), which interconnect the complexes into corrugated supramolecular layers parallel to the (b,c) plane. The coexistence of these ring motifs and $\pi-\pi$ stacking interactions (centroid−centroid = 4.392 Å) produces a highly ordered packing arrangement, where each pseudo-square-planar Co(II) center is linked to its neighbors through a network of weak C−H···C contacts and aromatic overlaps.[43]

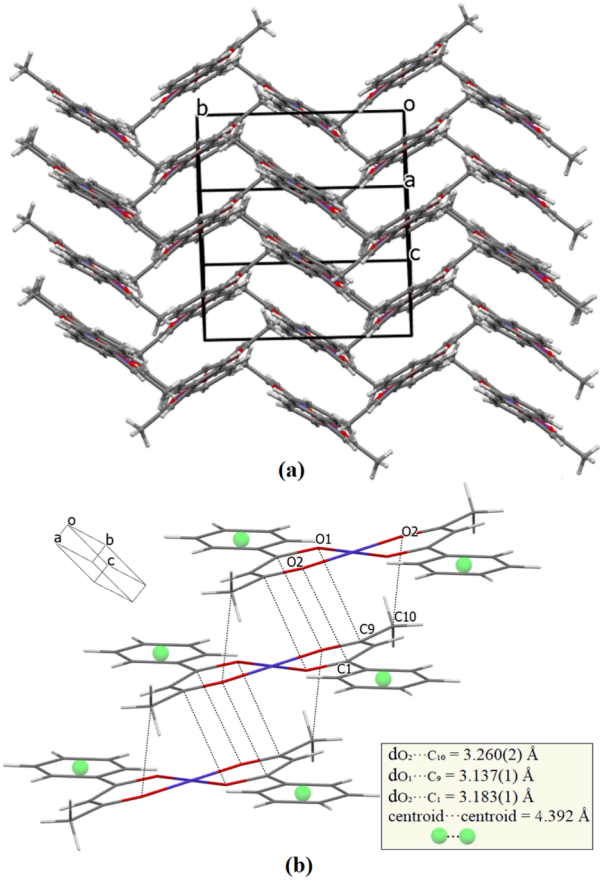

Figure 2. (a) Crystal packing of $[Co(bzac)_2]$, showing zigzag molecular layers parallel to the *(b,c)* plane. (b) $\pi-\pi$ stacking interactions between neighboring phenyl rings and illustration of $O_{lp}\cdots C\pi$ interactions between adjacent $[Co(bzac)_2]$ molecules.

Furthermore, Figure 3b shows the crystal packing of $[Co(bzac)_2]$ viewed along the *a*-axis, highlighting arrangement of discrete complexes within the monoclinic unit cell. The Co(II) centers occupy inversion centers and are coordinated by two chelating bzac ligands. The molecules are aligned along the *b*-axis and alternate in orientation, forming a dense and orderly packing.

Moreover, the molecular packing diagram (Figure 2b) reveals short O···C intermolecular contacts between adjacent $[Co(bzac)_2]$ units, with distances of 3.137−3.261 Å, slightly below the sum of the van der Waals radii. These contacts occur between the carbonyl and enolate oxygen atoms (O1, O2, O2′) and the β-diketonate carbon atoms (C9, C10) of neighboring molecules.[44] The geometric arrangement suggests a lone-pair−π interaction, where the oxygen lone pair interacts with the delocalized π system of the O−C = C−C = O chelate ring.[45,46] Such weak O···π contacts are frequently observed in β-diketonate frameworks and play a subtle yet stabilizing role in consolidating the zigzag supramolecular architecture of the crystal.[18]

3.2. Comparative Crystallographic Analysis Based on the CSD

A targeted CSD survey (v2025.3)[47] identified seven closely related $[M(bzac)_2]$ entries (Table 2) in which only the metal changes while the bzac ligand and O,O′ chelation motif are identical: Pb, Pd(trans), Pd(cis), Sn, Cu, Cu01, Cu02 with refcodes ZZZPQG,[48] PDPBTD,[49] PBONSN,[36] CBZACP,[50]

https://doi.org/10.1021/acs.inorgchem.5c05597
Inorg. Chem. 2026, 65, 3084−3101

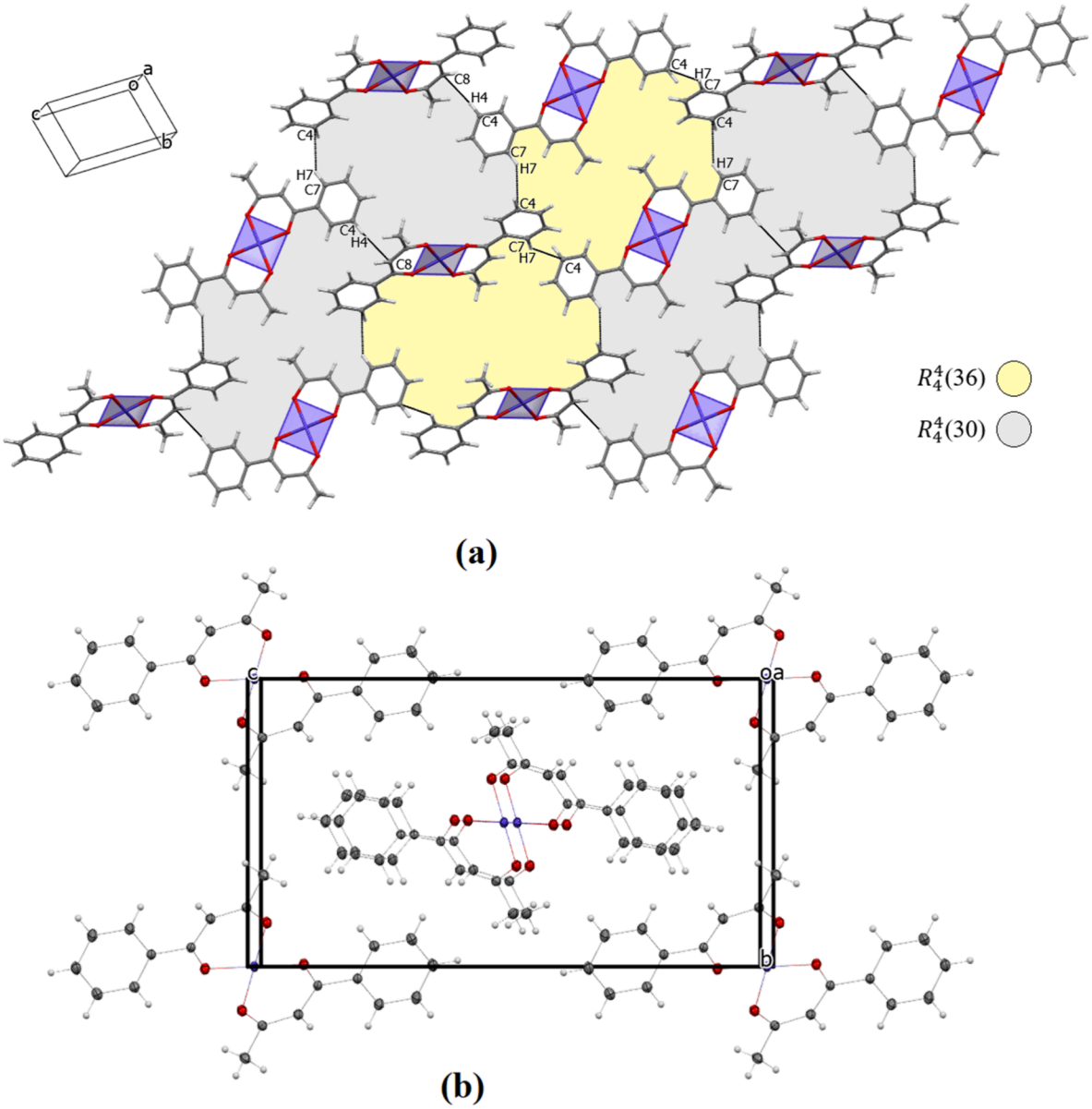

Figure 3. Supramolecular packing of $[Co(bzac)_2]$ (a) showing C−H···C interactions forming $R_4^4(30)$ (gray) and $R_4^4(36)$ (yellow) ring motifs that link the complexes into layers parallel to the (b,c) plane, And (b) viewed along the *a*-axis, showing the centrosymmetric Co(II) complexes arranged in alternating rows along the *b*-axis within the monoclinic unit cell.

Table 2. Crystallographic Comparison of $[M(bzac)_2]$ Complexes Reported in the CSD (v2025.3) and the Present $[Co(bzac)_2]$ Compound

complex	refcode	space group	geometry at M	M−O (Å)	molecular arrangement	year
$[Pb(bzac)_2]$	ZZZPQG	$P2_1an$	near-planar PbO_4 (holodirected)	nd[a]	nd[a]	1937
trans-$[Pd(bzac)_2]$	PDPBTD	$P2_1/c$	square-planar	1.965−1.965	layered packing along *b*	1967
$[Sn(bzac)_2]$	PBONSN	$C2/c$	hemidirected, pseudotrigonal-bipyramidal	2.138−2.294	slightly twisted chelate planes	1975
cis-$[Pd(bzac)_2]$	CBZACP	$P2_1/c$	square-planar	1.975−1.978	molecular stacking with stereochemically active lone pair	1976
$[Cu(bzac)_2]$	CUBEAC	$P2_1/c$	square-planar	1.914−1.931	discrete monomers; pseudolayered packing with Cu···C ≈ 3.02 Å	1966
$[Cu(bzac)_2]$	CUBEAC01	$P2_1/n$	square-planar	1.918−1.924	planar molecular stacking	2004
$[Cu(bzac)_2]$	CUBEAC02	$P2_1/c$	distorted square-planar	1.914−1.918	weak axial elongation depending on solvation	2019
$[Co(bzac)_2]$		$P2_1/n$	strictly square-planar	1.919−1.922	zigzag layers parallel to (b,c)	this work

[a]**Note:** No atomic coordinates are available for the early $Pb(bzac)_2$ report.

https://doi.org/10.1021/acs.inorgchem.5c05597
Inorg. Chem. 2026, 65, 3084−3101

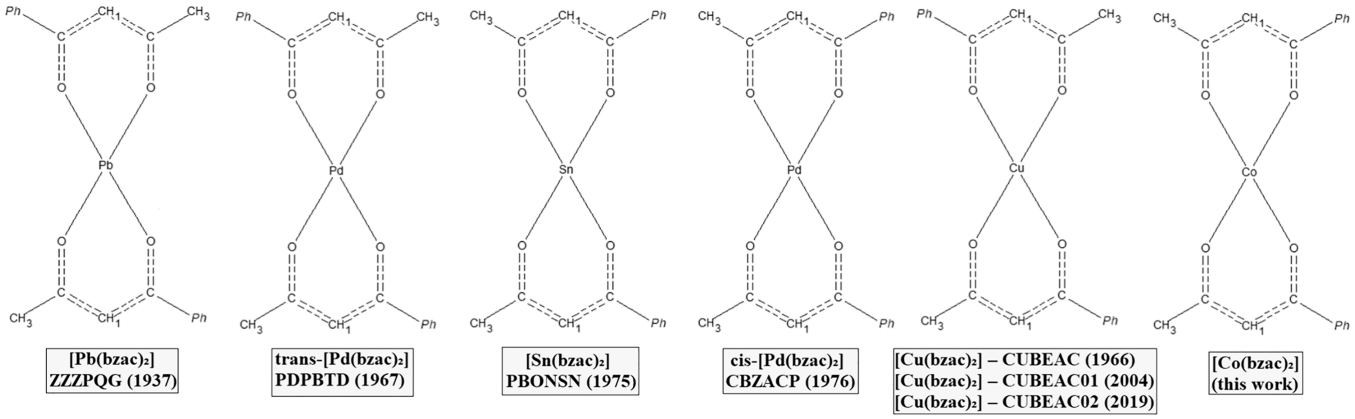

Figure 4. Chemical diagram of $[M(bzac)_2]$ analogues (M= Pb, Pd, Sn, Cu or Co) with corresponding CSD refcodes. $Pt(bzac)_2$.

Table 3. Key Noncovalent Interactions in the $[M(bzac)_2]$ Series (M = Co, Cu, Pd, Sn), Highlighting the Principal $\pi-\pi$, Metal$-\pi$, and C$-$H$\cdots\pi$ Contacts Extracted from the Crystal Structures

complex (CSD refcode)	key interaction type	atoms/rings involved	distance (Å)	structural significance
$[Co(bzac)_2]$ **(this work)**	$\pi-\pi$ stacking	centroid$\cdots$centroid	4.39	strong parallel stacking, generates columnar aromatic chains
	metal$\cdots$metal	Co1$\cdots$Co1	4.392	linear Co$\cdots$Co arrangement reinforcing the columns
	metal$\cdots$arene	Co1$\cdots$C3	3.27	short Co$\cdots\pi$ contact stabilizing the π-stack
	C$-$H$\cdots\pi$/C$\cdots$H	C4$\cdots$H7/H4$\cdots$C8	2.78$-$2.90	tight side contacts locking adjacent columns/stabilizing lateral packing
$[Sn(bzac)_2]$ **(PBONSN)**	$\pi-\pi$ stacking	centroid$\cdots$centroid	5.16	moderately slipped rings, weaker π-stacking
	metal$\cdots$arene	Sn1$\cdots$C4/Sn1$\cdots$C7	3.74$-$3.78	weak Sn$\cdots$C contacts contributing to layer cohesion
	C$\cdots$C	several aromatic C$\cdots$C	~3.30$-$3.40	packing dominated by dispersive C$\cdots$C interactions
trans-$[Pd(bzac)_2]$ **(PDPBTD)**	$\pi-\pi$ stacking	centroid$\cdots$centroid	5.74$-$5.88	long, highly slipped π-contacts; only moderate stacking
	metal$\cdots$arene	Pd1$\cdots$C1	3.75	weak Pd$\cdots\pi$ interaction
	C$\cdots$C	C8B$\cdots$C8	3.37	lateral aromatic contacts forming sheets
cis-$[Pd(bzac)_2]$ **(CBZACP)**	$\pi-\pi$ stacking	centroid$\cdots$centroid	5.21	shorter than trans, but still moderate and slipped
	metal$\cdots$arene	Pd1$\cdots$C13	3.30	strongest Pd$\cdots$C(arene) interaction in the Pd series
	C$\cdots$C	C14$\cdots$C20	3.41	edge$-$edge aromatic contacts stabilizing ribbons
$[Cu(bzac)_2]$ **(CUBEAC)**	$\pi-\pi$ stacking	centroid$\cdots$centroid	4.47	strong, compact face-to-face stacking.
	metal$\cdots$metal	Cu1$\cdots$Cu1	4.475	Cu$\cdots$Cu pathways parallel to aromatic columns
	metal$\cdots$arene	Cu1$\cdots$C4	3.01	very short Cu$\cdots\pi$ contact, highly stabilizing
	C$-$H$\cdots\pi$	H5B$\cdots$C4B/H5$\cdots$C4	~2.95	strong C$-$H$\cdots\pi$ contacts tightening the lattice
$[Cu(bzac)_2]$ **(CUBEAC01)**	$\pi-\pi$ stacking	centroid pairs	4.47	twin strong $\pi-\pi$ interactions, typical of Cu(bzac).
	metal$\cdots$arene	Cu1$\cdots$C3/Cu1$\cdots$C3B	3.37$-$3.44	Cu$\cdots\pi$ stabilization on both faces
	C$-$H$\cdots\pi$	H1B$\cdots$C10/H2$\cdots$C$\cdots$	~3.04	locks aromatic layers in 3D
$[Cu(bzac)_2]$ **(CUBEAC02)**	$\pi-\pi$ stacking	centroid pairs	4.47	same strong face-to-face stacking as CUBEAC
	metal$\cdots$arene	Cu1$\cdots$C10	3.02	robust Cu$\cdots\pi$ contact
	C$-$H$\cdots\pi$	H17$\cdots$C$\cdots$/H19$\cdots$C$\cdots$	2.93$-$2.94	shortest H$\cdots$C contacts of all Cu complexes

CUBEAC,[51] CUBEAC01[52] and CUBEAC02,[53] respectively (Figure 4). Crystallographically, all these structures share a mononuclear, nonpolymeric $[M(bzac)_2]$ framework stabilized by bidentate O,O′ chelation and the typical β-diketonate six-membered chelate ring. However, the coordination geometry and supramolecular arrangement evolve systematically with the metal center.

The lead(II) analogue corresponds to an early X-ray study. The space-group notation matches the standard setting $P2_1an$ (equivalent to the nonstandard *Pcn* cited by Cox et al.[48]), and the reported pseudohalving is consistent with an approximately planar O,O′-chelated PbO_4 environment (holodirected Pb(II)). However, the crystallographic atomic coordinates for this structure were not deposited in the original study and remain unavailable in the CCDC

In trans-$[Pd(bzac)_2]$ ($P2_1/c$), a square-planar PdO_4 motif is observed (d^8). Further, the Pd and the four oxygen atoms are strictly coplanar by symmetry (Pd$-$O ≈ 1.97 Å), forming layers parallel to the *b*-axis. The cis isomer, later characterized by Okeya et al. in 1976,[50] retains the same bzac bite geometry but displays a subtle torsion of the phenyl substituents, highlighting ligand$-$ligand steric torsion within an otherwise square-planar PdO_4 core.

The tin(II) analogue[36] shows a distorted pseudotrigonal bipyramidal geometry (Sn$-$O(eq) 2.135 Å, Sn$-$O(ax) 2.290 Å), with the lone pair occupying an equatorial position, confirming the stereochemical activity of Sn(II) and explaining the molecular (nonbridged) packing observed in C_2/c.

For copper(II), several $[Cu(bzac)_2]$ structures confirm a consistent mononuclear square-planar coordination modulated slightly by crystal packing and solvation. The earliest, reported by Hon et al.,[51] presents discrete monomers ($P2_1/c$) where Cu and the four O atoms are coplanar, forming short Cu$\cdots$C intermolecular contacts (~3.02 Å) that support a pseudolayered

https://doi.org/10.1021/acs.inorgchem.5c05597
Inorg. Chem. 2026, 65, 3084−3101

Table 4. Comparative Structural and Electronic Features of the $[M(bzac)_2]$ Series

metal center (Year)	electronic configuration	dominant stereochemical/ligand-field effect	key supramolecular/intermolecular interactions	electronic & optical implications
Pb(II) (1937)	$6s^2\ 6p^0$	inert-pair effect → holodirected coordination (inactive lone pair)	weak dispersion-driven contacts; no directional $\pi-\pi$ stacking	minimal covalency; electronic isolation of metal; weak optical activity
Sn(II) (1975)	$5s^2\ 5p^0$	active s^2 lone pair → hemidirected geometry	asymmetric packing; absence of $\pi-\pi$ overlap	strong stereochemical distortion; low conjugation; poor delocalization
Pd(II) (trans) (1967)	$4d^8$	ligand-field stabilization → perfect square-planar PdO_4	layered packing ‖ b; Pd and O coplanar by symmetry	high orbital overlap; strong M−O π back-bonding; intense LMCT absorption
Pd(II) (cis) (1976)	$4d^8$	same field as trans; steric torsion of phenyls	weak interlayer $\pi-\pi$; limited planarity	reduced delocalization due to ligand torsion
Cu(II) (1966)	$3d^9$	Jahn−Teller axial lability; dx^2-y^2 ground state	layer-like packing; short Cu···C contacts (~3.0 Å)	partial electronic delocalization; moderate optical anisotropy
Cu(II) (2004)	$3d^9$	same field, minor axial strain; solvent-free form	discrete monomers; no polymerization	stable planar field; reproducible optical response
Cu(II) (2019)	$3d^9$	solvent coordination controls geometry (5-coord. ↔ 4-coord.)	$\pi-\pi$ and H-bonding modulated by solvent inclusion	solvent-dependent color, variable absorption edges
Co(II) (this work)	$3d^7$	ligand-field stabilization under inversion symmetry	zigzag $\pi-\pi$ stacking (centroid−centroid = 4.39 Å); C−H···O & C−H···C motifs	enhanced $\pi-\pi$ coupling and charge delocalization; potential optical and semiconducting behavior

packing. A later study by Dey et al.[52] also reported a monomeric $Cu(bzac)_2$ complex with an identical O,O′ chelating mode and square-planar CuO_4 coordination, confirming the reproducibility of this motif across synthetic routes. More recently, Krishnegowda et al.[53] described two solvent-dependent variants: a desolvated $Cu(bzac)_2$ remaining perfectly square-planar, and a methanol-solvated analogue adopting a slightly distorted square-pyramidal geometry due to weak axial coordination by solvent molecules. Collectively, these findings demonstrate that all $Cu(bzac)_2$ derivatives are mononuclear and nonpolymeric, preserving the O,O′-chelating β-diketonate topology while expressing the inherent axial lability of Cu(II) within this ligand field.

To provide a clearer crystallographic comparison across these derivatives, Table 2 summarizes the essential structural parameters—including space group, coordination geometry, and molecular packing—for all $[M(bzac)_2]$ analogues retrieved from the CSD alongside the present $[Co(bzac)_2]$ compound.

In comparison, the present $[Co(bzac)_2]$ complex preserves the same O,O′-chelating motif while featuring a centrosymmetric four-coordinate CoO_4 core. Its molecular packing contrasts with the planar stacking observed for the Pd(II) and Cu(II) analogues and with the axially distorted geometry found in Sn(II) derivatives. These structural features clearly indicate that the cobalt compound adopts a strictly square-planar coordination environment, in sharp contrast to the pseudobipyramidal configuration characteristic of Sn(II) β-diketonates. Overall, the comparison across the $[M(bzac)_2]$ family reveals that while the bzac chelating topology remains invariant, the metal-dependent stereochemistry governs both the degree of planarity and the supramolecular cohesion, making $[Co(bzac)_2]$ a crystallographically significant intermediate within this classical β-diketonate series.

3.3. Comparative Analysis of Noncovalent Interaction Networks across the $[M(bzac)_2]$ Series

In order to place the structural features of the new Co(II) derivative into a broader supramolecular context, we benchmarked its noncovalent interaction framework against the full $[M(bzac)_2]$ series, enabling a metal-resolved comparison of π-stacking efficiency, metal-arene engagement, and secondary contacts. As summarized in Table 3, comparison of the noncovalent contact patterns across the $[M(bzac)_2]$ series (M = Co, Cu, Pd, Sn) reveals a clear and systematic metal dependence of the supramolecular architecture. The Co(II) and Cu(II) derivatives exhibit the shortest centroid···centroid separations and the most compact metal···arene approaches, leading to tightly packed columnar stacks in which chelate planes and phenyl rings are efficiently π-locked. In $[Co(bzac)_2]$, the combination of strong $\pi-\pi$ stacking and relatively short Co···C(arene) and C−H···π contacts generates highly coherent one-dimensional aromatic columns, with Co···Co vectors running parallel to the stacking direction. The various $Cu(bzac)_2$ structures preserve essentially the same packing motif, with Cu···π interactions that are slightly shorter than in the Co analogue and additional C−H···π links that rigidify the columns and cross-link them laterally. Together, these features point to a more strongly interconnected, anisotropic lattice for the Co and Cu complexes, in which the metal center not only defines the local chelate geometry but also amplifies long-range cohesion via efficient mediation of π-stacking.

In contrast, the Sn(II) and Pd(II) congeners display weaker and more diffuse noncovalent networks. For PBONSN, the $Sn(bzac)_2$ framework is dominated by longer, more slipped $\pi-\pi$ contacts and relatively soft Sn···C(arene) approaches, so that aromatic layers are maintained primarily by dispersive C···C contacts rather than by directed metal-assisted stacking. The two Pd(II) structures further illustrate the sensitivity of the supramolecular landscape to both the metal and the cis/trans arrangement: the trans-Pd complex features the longest and most offset $\pi-\pi$ contacts of the series and only modest Pd···π engagement, while the cis-Pd is able to support a somewhat more compact Pd···arene approach but still lacks the dense, columnar connectivity observed for Co and Cu. Overall, the evolution from Sn and Pd to Co and Cu corresponds to a progressive reinforcement and directionalisation of the noncovalent interaction manifold, with Co(II) and Cu(II) sitting at the strongly stacked, structurally coherent end of the series. This metal-dependent modulation of $\pi-\pi$, metal···π and C−H···π contacts provides a structural rationale for the distinctive packing anisotropy and morphological behavior discussed for $[Co(bzac)_2]$, and underpins the structure−property correlations we draw for this compound within the broader $[M(bzac)_2]$ family.

https://doi.org/10.1021/acs.inorgchem.5c05597
Inorg. Chem. 2026, 65, 3084−3101

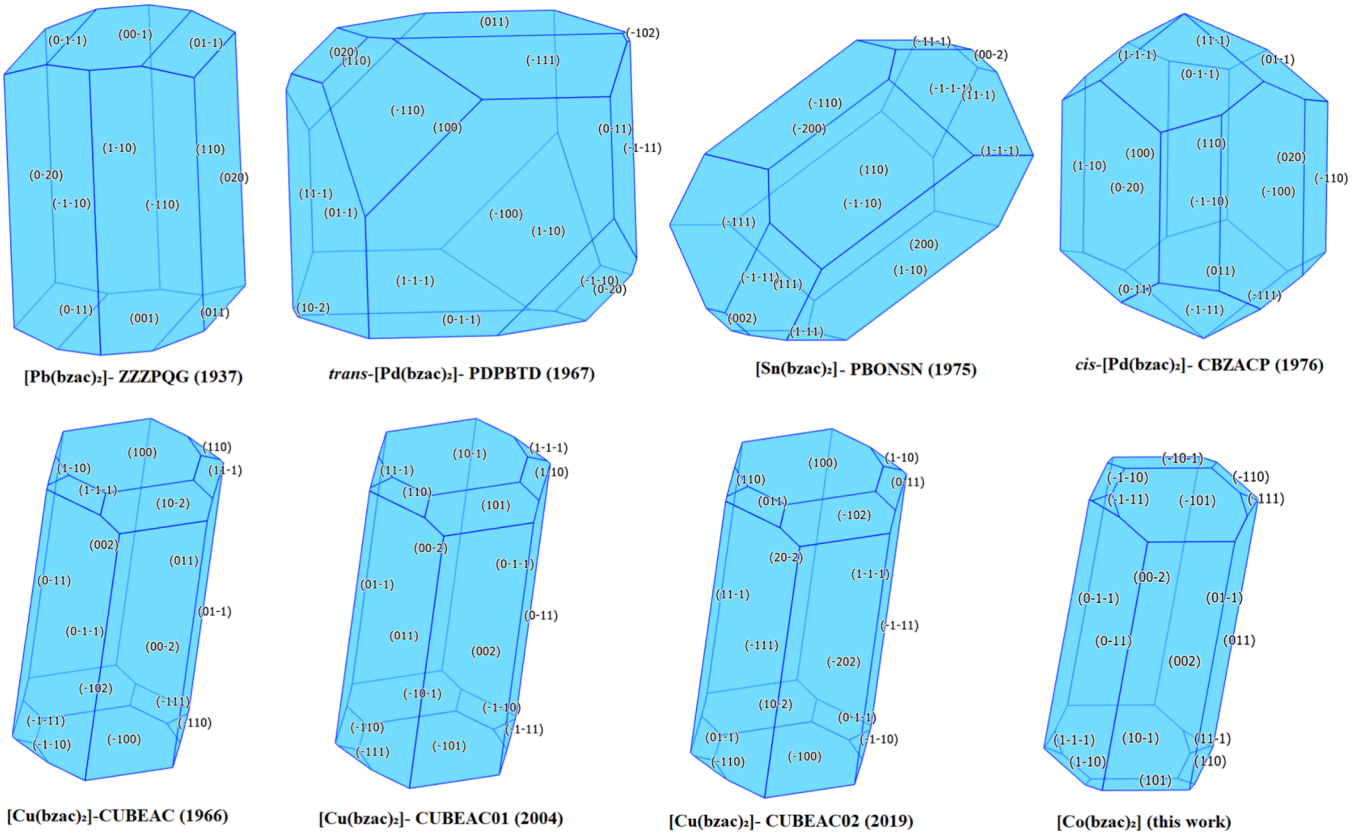

Figure 5. Predicted BFDH morphologies of the $[M(bzac)_2]$ (M = Pb, Pd, Sn, Cu, Co) series generated from single-crystal data.

3.4. Comparative Analysis of Structural, Electronic, and Supramolecular Trends in the $[M(bzac)_2]$ Family

Beyond their crystallographic similarities, the $[M(bzac)_2]$ complexes display a progressive modulation of geometry, bonding, and supramolecular organization that mirrors the changing electronic configuration of the metal center. The comparative behavior across Pb(II), Pd(II), Sn(II), Cu(II), and Co(II) analogues reveals a coherent evolution from stereochemically active lone-pair distortion to rigid square-planar symmetry (Table 4).

The Pb(II) and Sn(II) derivatives illustrate the classical contrast between *holodirected* and *hemidirected* coordination geometries, governed by the inert-pair effect. In $Pb(bzac)_2$, the $6s^2$ lone pair remains largely inert, producing a near-planar valence distribution consistent with early structural interpretations. In contrast, $Sn(bzac)_2$ shows an explicitly *hemidirected* environment: the $5s^2$ lone pair occupies an equatorial region, generating a pseudotrigonal-bipyramidal geometry with unequal Sn−O distances ($\Delta \approx 0.15$ Å). This stereochemical activity introduces a directional bias in the packing and breaks the planarity typical of d^8 or d^9 transition-metal analogues.

The Pd(II) and Cu(II) complexes, both stabilized by strong O,O′ chelation, exemplify classical ligand-field trends within β-diketonate frameworks. For Pd(II) (d^8), the *square-planar* PdO_4 core is perfectly coplanar, leading to the highest degree of covalent delocalization and minimal structural strain. The Cu(II) (d^9) analogues preserve this geometry but reveal a subtle *Jahn−Teller-driven axial lability*: in desolvated crystals, Cu remains strictly square-planar, whereas weak axial Cu−O contacts emerge upon solvation, lengthening to 2.3−2.4 Å and slightly distorting the planar field. These fine variations in Cu(II) coordination demonstrate how the antibonding character of the dz^2 orbital modulates the molecular symmetry.

Compared with these soft d^8/d^9 centers, the Co(II) complex reported herein displays a particularly stable *square-planar* CoO_4 configuration (Co−O ≈ 1.92 Å), maintained even at 100 K. The Co atom lies on an inversion center, ensuring perfect trans alignment and a negligible deviation from planarity. This centrosymmetric arrangement suppresses axial interactions and promotes uniform $\pi-\pi$ stacking between nearly coplanar phenyl rings (centroid−centroid = 4.39 Å). The packing thus combines the rigidity of a square-planar d^7 core with the delocalized character of β-diketonate π-systems, leading to an extended zigzag supramolecular network reminiscent of the Pd and Cu analogues but electronically more delocalized.

A remarkable feature emerging from this comparison is the gradual enhancement of $\pi-\pi$ communication from Sn → Cu → Co. While the Sn(II) compound lacks continuous aromatic overlap due to the lone-pair distortion, both Cu(II) and Co(II) exhibit centroid separations typical of efficient $\pi-\pi$ stacking (3.9−4.4 Å). The increased coplanarity in $Co(bzac)_2$ maximizes this overlap, potentially enabling charge or exciton migration along the stacking direction. Such structural organization provides a rationale for the optical and photophysical properties often reported for transition-metal β-diketonates.

In summary, the $[M(bzac)_2]$ family exemplifies a continuous transition from *stereochemically active lone pairs* (Sn, Pb) to *ligand-field-stabilized planarity* (Pd, Cu, Co). The evolution of geometry, bond metrics, and packing parallels the increasing participation of d orbitals in M−O π bonding. Within this continuum, the present Co(II) complex represents an intermediate but electronically distinct species—combining high planarity with significant $\pi-\pi$ interaction density—making

https://doi.org/10.1021/acs.inorgchem.5c05597
Inorg. Chem. 2026, 65, 3084−3101

Table 5. Morphology–Structure Correlation within the $[M(bzac)_2]$ Series

complex refcode year	dominant faces (BFDH)	characteristic crystal habit	main directional interactions	growth anisotropy/ elongation	structural–morphological correlation
$[Pb(bzac)_2]$ ZZZPQG (1937)	{110},{001}, {011}	prismatic, nearly isometric	weak van der Waals and O···C(lp···π)	very low	isotropic growth due to lone-pair repulsion and absence of strong π-stacking
trans-$[Pd(bzac)_2]$ PDPBTD (1967)	{100}, {110}, {011}	flattened polyhedron	$\pi-\pi$ and C–H···O within layers	moderate (2D)	compact morphology governed by planar coordination and tight packing
$[Sn(bzac)_2]$ PBONSN (1975)	{110}, {200}, {002}	elongated bipyramidal	O···C(lp···π) and C–H···O	moderate	slight elongation along [001] induced by asymmetric coordination and lone pair
cis-$[Pd(bzac)_2]$ CBZACP (1976)	{100}, {110}, {011}	compact prismatic	symmetric C–H···O, weak $\pi-\pi$	low	symmetric cis-configuration reduces anisotropy; denser 3D packing
$[Cu(bzac)_2]$ CUBEAC (1966)	{001}, {011}, {100}	prismatic, slightly elongated	$\pi-\pi$ stacking and O··· C(lp···π)	high	onset of 1D growth along [001] direction
$[Cu(bzac)_2]$ CUBEAC01 (2004)	{002}, {011}, {10–1}	acicular	$\pi-\pi$ stacking reinforced by axial elongation	very high	strong directional packing enhances anisotropy; needle-like habit
$[Cu(bzac)_2]$ CUBEAC02 (2019)	{100}, {10– 1}, {011}	needle-like (acicular)	cooperative $\pi-\pi$ and C–H···O	extreme	solvation promotes 1D propagation and face-selective growth
$[Co(bzac)_2]$ **this work**	{002}, {011}, {10–1}	highly acicular, elongated along [001]	$\pi-\pi$ stacking and O···C(lp···π)	extreme	maximum anisotropy driven by strong planar conjugation and directional stacking

it a structurally and electronically pivotal member of the $[M(bzac)_2]$ series.

3.5. Comparative Morphological Analysis of $M(bzac)_2$ Complexes

The calculated BFDH morphologies (Figure 5) of the isostructural β-diketonate complexes $[M(bzac)_2]$ (M = Pb, Pd_trans, Pd_cis, Sn, Cu, Co) provide valuable insights into the influence of the metal center on the crystal growth anisotropy and the final crystal habit. For all complexes, the experimental faces used for comparison correspond to the dominant low-index crystallographic planes identified from single-crystal X-ray diffraction data and, where available, from reported macroscopic crystal habits in the original structure determinations. The comparison with the BFDH-predicted morphologies is therefore qualitative in nature and is based on the presence, symmetry, and relative prominence of these experimentally observed faces, rather than on absolute growth rates or surface energy calculations. This approach allows a consistent assessment of growth anisotropy across the $[M(bzac)_2]$ series while maintaining direct correspondence between crystallographic structure, supramolecular packing, as reflected in the external crystal morphology. Despite their structural analogies, marked morphological variations are observed, which can be directly correlated to the metal–oxygen coordination environment and the molecular packing forces dominating in each lattice (Table 5).

$[Pb(bzac)_2]$ – ZZZPQG (1937). The lead(II) compound displays an isometric prismatic morphology, dominated by the {110}, {001}, and {011} faces. The nearly equant habit reflects the stereochemically active lone pair of Pb^{2+}, which distorts the coordination environment but simultaneously distributes intermolecular contacts isotropically. The absence of strong directional $\pi-\pi$ or C–H···O interactions results in limited anisotropy.

Trans-$[Pd(bzac)_2]$ – PDPBTD (1967). The trans-palladium(II) complex exhibits a flattened polyhedral morphology with major {100}, {110}, and {011} faces. This compact form arises from the square-planar geometry of PdO_4 and the strong intralayer $\pi-\pi$ stacking between benzoylacetonate ligands, which promotes dense packing within the (100) plane and limits elongation. The morphology thus mirrors its high planarity and reduced three-dimensional connectivity.

$[Sn(bzac)_2]$ – PBONSN (1975). The tin(II) derivative reveals a slightly elongated bipyramidal habit characterized by dominant {110}, {200}, and {002} faces. This shape originates from the pseudotrigonal-bipyramidal geometry of Sn(II), where the stereochemically active lone pair drives a weak anisotropy along the [001] direction. The elongation corresponds to the alignment of secondary O···C(lp···π) interactions guiding the crystal growth.

Cis-$[Pd(bzac)_2]$ – CBZACP (1976). The cis-Pd(II) complex adopts a compact prismatic morphology, distinct from its trans analogue by the presence of equivalent faces {100}, {110}, and {011}. The cis arrangement of the chelates generates a more symmetrical distribution of short C–H···O and $\pi-\pi$ interactions, producing a less flattened but more isometric habit, consistent with a nearly planar PdO_4 chromophore slightly twisted by ligand–ligand repulsion.

$[Cu(bzac)_2]$ – CUBEAC (1966); CUBEAC01 (2004); CUBEAC02 (2019). The three Cu(II) structures show a remarkable evolution in morphological anisotropy through time, while maintaining similar structural topology.

- CUBEAC (1966) displays an elongated prismatic morphology along [001], with dominant {001}, {011}, and {100} faces.
- CUBEAC01 (2004) presents a sharper acicular habit, in which growth along [001] becomes more pronounced due to stronger $\pi-\pi$ stacking interactions and axial elongation of the CuO_4 chromophore.
- CUBEAC02 (2019) exhibits the most needle-like (acicular) morphology, where the enhanced contribution of the {100} and {10–1} faces correlates with cooperative C–H···O and O···C(lp···π) interactions that favor one-dimensional propagation.The progressive elongation within this series reflects subtle packing reinforcement along [001], revealing how minor changes in lattice energy or π-overlap can profoundly affect crystal growth directions.

$[Co(bzac)_2]$ (This Work). The newly synthesized cobalt(II) complex displays a distinctly acicular habit elongated along the [001] direction, dominated by the {002}, {011}, and {10–1} faces. The strong anisotropy parallels the orientation of $\pi-\pi$ stacking between benzoylacetonate rings and lone-pair···π O···C interactions that propagate through the lattice. This anisotropy explains the experimentally observed needle-like blue crystals,

https://doi.org/10.1021/acs.inorgchem.5c05597
Inorg. Chem. 2026, 65, 3084–3101

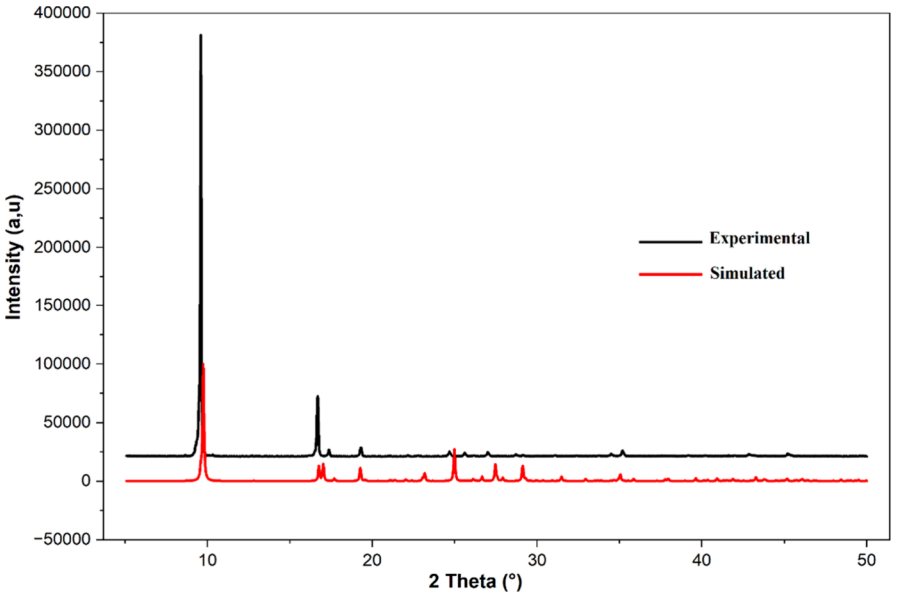

Figure 6. Experimental powder X-ray diffraction pattern of $[Co(bzac)_2]$ (black), compared with the pattern simulated from the single-crystal structure (red). The excellent agreement in peak positions confirms the bulk phase purity and the correspondence between the microcrystalline sample and the SC-XRD model.

confirming the reliability of the BFDH prediction when compared with the experimentally observed dominant faces inferred from single-crystal data and macroscopic crystal habit. The morphological similarity with the Cu(II) analogues suggests comparable square-planar coordination and stacking-driven anisotropic growth.

3.5.1. Morphology−Structure Correlation and Comparative Discussion. The morphological sequence follows the order of increasing anisotropy: Pb ≈ cis-Pd < trans-Pd < Sn < Cu < Co. This progression directly reflects the balance between coordination geometry, electronic configuration, and supramolecular packing forces. Complexes with highly planar M−O frameworks (Pd, Cu, Co) tend to favor layered or one-dimensional growth, leading to acicular morphologies, whereas those with active lone pairs (Pb, Sn) generate more isotropic shapes due to steric distortion and multidirectional secondary interactions.

The comparative BFDH morphological study of the eight $[M(bzac)_2]$ compounds clearly demonstrates that the nature of the central metal ion governs the anisotropy of crystal growth through its coordination geometry and intermolecular interaction network.

The newly obtained $Co(bzac)_2$ shows the most pronounced elongation, attributed to cooperative $\pi-\pi$ stacking and O···C(lp···π) contacts guiding growth along [001], thus bridging the structural and morphological behavior observed for Cu(II) analogues. This finding reinforces the intrinsic link between electronic structure, supramolecular architecture, and external crystal morphology, validating the predictive accuracy of the BFDH model in metal−β-diketonate systems.

3.6. Powder X-ray Diffraction and Bulk Phase Purity

The room-temperature PXRD pattern of $[Co(bzac)_2]$ is shown in Figure 6, together with the pattern simulated from the single-crystal structure refined in $P2_1/n$. The experimental diffractogram displays a dominant reflection at 2θ = 9.60° (I/I_{max} = 100%), accompanied by an adjacent shoulder at 9.26° (2.9% relative intensity) and a series of weaker peaks at 16.68° (14.5%), 19.32°, 24.68°, 27.00° and 35.18°. Within the experimental resolution, all of these reflections match those expected for the monoclinic cell determined by SC-XRD, and no additional peaks are detected over the 5−50° range. This firmly establishes that the bulk microcrystalline sample is a single phase corresponding to the $[Co(bzac)_2]$ structure.

Using the lattice parameters obtained from SC-XRD (Table 1), the most intense reflection at 2θ = 9.60° can be indexed as the (002) plane [d(002) ≈ 9.19 Å], which corresponds to the repeat distance along the crystallographic *c* axis. This assignment is fully consistent with the layered packing of nearly planar $[Co(bzac)_2]$ molecules described above: the π-stacked benzoylacetonate ligands and CoO_4 chromophores form corrugated sheets parallel to the (b,c) plane, and the periodic separation of these layers along *c* gives rise to the strong low-angle (002) reflection. Higher-angle peaks at 16.68°, 19.32°, 24.68°, 27.00° and 35.18° can be associated with higher-index lattice planes such as (0 1 3), (0 2 2), (1 1 2) and (1 3 2), which probe more complex combinations of in-plane and interlayer correlations within the same zigzag framework.

The excellent agreement between the experimental and simulated patterns, both in peak positions and in the overall profile, demonstrates that the structural motifs revealed by SC-XRD—strictly square-planar CoO_4 coordination, nearly coplanar benzoylacetonate ligands, and zigzag stacks of molecules along the [001] direction—are faithfully reproduced throughout the bulk. Small discrepancies in relative intensities are readily attributed to preferred orientation, as expected for samples composed of strongly elongated, needle-like crystals: partial alignment of the long axes enhances reflections associated with planes perpendicular to the growth direction (such as (002)) while slightly attenuating others.

From a structure−property standpoint, the PXRD results close the loop between local coordination, supramolecular organization, and macroscopic morphology. The intense (002) reflection at low angle directly reflects the long-range periodicity of the stacked molecular layers that also control the BFDH-predicted crystal habit. In other words, the same planar CoO_4/β-diketonate architecture that enforces a highly anisotropic

https://doi.org/10.1021/acs.inorgchem.5c05597
Inorg. Chem. 2026, 65, 3084−3101

Table 6. Quantitative Descriptors of Chelate Planarity and Coordination Symmetry in $M(bzac)_2$ Complexes

complex	CSD refcode	$RMSD_{chelate}$ (Å)	$\Delta(M-O_4$ plane) (Å)	$\varphi_{chelate-phenyl}$ (°)	φ_{inter} (°)	planarity
$Pb(bzac)_2$	ZZZPQG	nd[a]	nd[a]	nd[a]	nd[a]	nearly planar (C_{2v}-like pseudosymmetry)
$Sn(bzac)_2$	PBONSN	0.002	1.02	30.5	75.5	hemidirected/distorted
trans-$Pd(bzac)_2$	PDPBTD	0.006	0.000	23.5	0.0	highly planar
cis-$Pd(bzac)_2$	CBZACP	0.027/0.002 (A/B)	0.036	17/41 (A/B)	12.7	planar
$Cu(bzac)_2$	CUBEAC	0.022	0.000	16.1	0.0	planar
$Cu(bzac)_2$	CUBEAC01	0.011	0.000	5.9	0.0	planar
$Cu(bzac)_2$	CUBEAC02	0.007	0.000	7.4	0.0	slightly distorted
$Co(bzac)_2$ (this work)		0.038	0.000	12.15	0.0	highly planar

[a]No crystallographic atomic coordinates (x, y, z) were deposited for ZZZPQG ($Pb(bzac)_2$).The original X-ray report (Cox, Webster & Wardlaw, 1937)[48] states that the molecule "very nearly has C_{2v} symmetry", which is only possible for a nearly planar configuration. Therefore, $Pb(bzac)_2$ is classified as *nearly planar*, although quantitative planarity metrics (RMSD, $\Delta(M-O_4)$, dihedral angles) cannot be computed.

packing motif is simultaneously responsible for (i) the dominant low-angle scattering in the PXRD pattern and (ii) the experimentally observed acicular growth along [001]. This coherent picture confirms that the morphological anisotropy of $[Co(bzac)_2]$ is an intrinsic consequence of its crystallographic design rather than a kinetic artifact of crystallization conditions.

3.7. Quantitative Planarity Metrics for the β-Diketonate Chelate

In order to address quantitatively the "nearly planar" description of $[M(bzac)_2]$ complexes, we extracted from the CSD a consistent set of geometrical metrics (Table 6): (i) the root-mean-square deviation of the O−C−C−C−O chelate backbone from its least-squares plane, $RMSD_{chelate}$; (ii) the displacement of the metal from the O_4 mean plane, $\Delta(M-O_4)$; (iii) the dihedral angle between the chelate and the appended phenyl ring, $\varphi_{chelate-phenyl}$; and (iv) the interchelate dihedral angle, $\varphi_{(inter)}$, which measures the mutual twist of the two β-diketonate ligands. Taken together, these parameters probe both the local distortion of the O_2C_2 skeleton and the extent to which the π-conjugated benzoylacetonate fragments remain coplanar around the metal center.

Within this framework, the hemidirected $Sn(bzac)_2$ complex (PBONSN) exhibits an almost perfectly flat O−C−C−C−O fragment ($RMSD_{chelate}$ = 0.002 Å) but a large $\Delta(Sn-O_4)$ displacement of 1.02 Å and a very large $\varphi_{inter} \approx 75.5°$, consistent with a strongly distorted coordination sphere despite the formally planar ligand. The cis-$Pd(bzac)_2$ derivative (CBZACP) displays two crystallographically independent molecules with significantly different planarity metrics ($RMSD_{chelate}$ = 0.027/0.002 Å; $\varphi_{chelate-phenyl}$ = 17/41° and φ_{inter} = 12.7°), reflecting packing-induced bending of both the chelate backbone and the aryl rings. In contrast, the trans-$Pd(bzac)_2$ analogue (PDPBTD) and the $Cu(bzac)_2$ polymorphs (CUBEC, CUBEA01, CUBEA02) all show a strictly planar $M-O_4$ core [$\Delta(M-O_4)$ = 0.000 Å] and mutually eclipsed chelates (φ_{inter} = 0°), with small but nonzero chelate puckering ($RMSD_{chelate} \leq 0.022$ Å) and modest phenyl tilts (5.9−16.1°), which justify their classification as planar or only slightly distorted.

Our $[Co(bzac)_2]$ complex lies at the high-planarity end of this series. It combines a perfectly coplanar CoO_4 core [$\Delta(Co-O_4)$ = 0.000 Å] with an exactly eclipsed arrangement of the two β-diketonate ligands (φ_{inter} = 0°) and a relatively small chelate−phenyl twist ($\varphi_{chelate-phenyl}$ = 12.15°). Although the $RMSD_{chelate}$ value (0.038 Å) is slightly larger than for some Cu and Pd analogues, this deviation remains extremely small on an absolute scale and corresponds mainly to a subtle, nearly symmetric "breathing" of the O−C−C−C−O fragment rather than to a genuine out-of-plane buckle. From the perspective of the extended π-conjugated pathway encompassing the chelate and phenyl rings, $[Co(bzac)_2]$ therefore resides among the most planar members of the $[M(bzac)_2]$ family, in excellent agreement with its highly faceted, plate-like BFDH morphology and with the minimal splitting of the frontier π-orbitals revealed by our DFT calculations.

For completeness, $Pb(bzac)_2$ (ZZZPQG) is also included qualitatively in Table 3. No atomic coordinates (x, y, z) are available for this early structure; however, the original crystallographic report already emphasized that the molecule "very nearly has C_{2v} symmetry", which is only compatible with a nearly planar configuration. We therefore classify $Pb(bzac)_2$ as nearly planar, while indicating that quantitative planarity metrics ($RMSD_{chelate}$, $\Delta(M-O_4)$, dihedral angles) cannot be computed for this case.

3.8. Spectroscopic Characterization of $[Co(bzac)_2]$

3.8.1. FT-IR Analysis. The infrared spectrum of $[Co(bzac)_2]$ (Figure 7) exhibits the characteristic vibrational

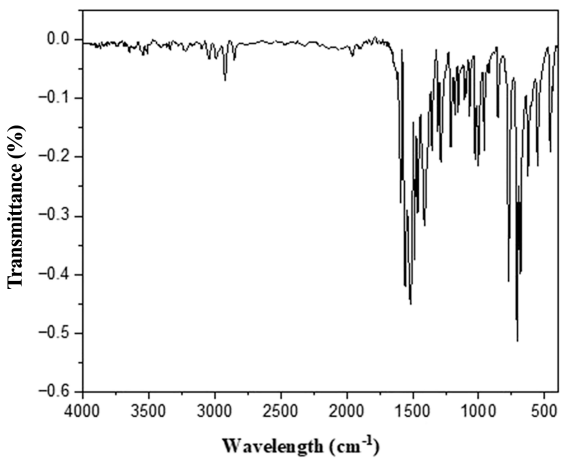

Figure 7. FTIR spectrum of complex $[Co(bzac)_2]$.

features of the β-diketone coordination environment.[54] The strong absorption band observed at ≈1610−1620 cm^{-1} is assigned to the ν(C = O) stretching vibration of the enolized β-diketonate group, while the band at ≈1520 cm^{-1} corresponds to the ν(C = C) stretching mode of the chelate ring.[55] The disappearance of the sharp carbonyl band typical of the free ligand near 1700 cm^{-1} and the simultaneous emergence of these two distinct absorptions confirm the enolization and O,O′-bidentate coordination of the bzac ligand to the Co(II) center.[9] Additional bands appearing around 1250−1270 cm^{-1} and 1170

https://doi.org/10.1021/acs.inorgchem.5c05597
Inorg. Chem. 2026, 65, 3084−3101

cm^{-1} can be assigned to C−O stretching vibrations, further supporting metal−oxygen bond formation through the oxygen donor atoms.[56] The medium-intensity band observed near 520−530 cm^{-1} is characteristic of the ν(Co−O) stretching mode, consistent with a square-planar CoO_4 coordination environment evidenced by the X-ray data. These IR observations therefore fully corroborate the crystallographic findings, confirming the chelation of the ligand through both oxygen atoms and the planar geometry around the cobalt center.

3.8.2. UV−Vis Absorption Analysis. The UV−Vis spectrum of [Co(bzac)$_2$] (Figure 8) was recorded in methanol

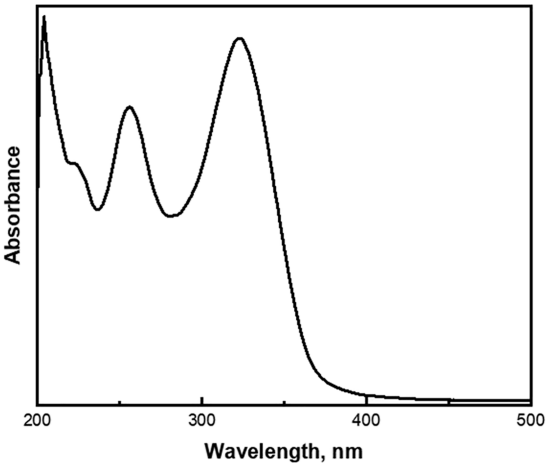

Figure 8. UV−vis spectrum of complex [Co(bzac)$_2$].

solution within the 190−500 nm range. The compound exhibits an intense absorption band in the UV region at ≈ 280−290 nm, attributed to $\pi\rightarrow\pi^*$ transitions localized within the conjugated benzoyl-acetone (bzac) moiety.[57] A shoulder of moderate intensity extending over ≈ 340 and 380 nm can be assigned to $n\rightarrow\pi^*$ transitions involving the nonbonding orbitals of the oxygen atoms.[18] Within the recorded range, the visible response appears only as a very weak, broad tail approaching 480−500 nm, which is compatible with a Laporte-forbidden, metal-centered d−d transition expected for square-planar Co(II) in a D_4h-like ligand field.[58] The overall spectral profile—dominant ligand-based $\pi\rightarrow\pi^*$/$n\rightarrow\pi^*$ features with only a faint low-energy tail—matches the electronic structure inferred from the FMO analysis and the square-planar CoO_4 geometry determined crystallographically. These spectroscopic results, in excellent agreement with the X-ray and comparative CSD analyses, validate the coordination mode and confirm the structural integrity of the [Co(bzac)$_2$] complex.

3.9. Theoretical Calculations

The optimized molecular structure of [Co(bzac)$_2$] retains the planarity of the CoO_4 chromophore and the inversion symmetry of the metal site observed experimentally (space group $P2_1/n$). Excellent agreement is achieved between the calculated and experimental geometrical parameters (Table 7). The Co−O bond lengths are slightly shorter in the gas-phase model (1.790−1.796 Å) than in the solid state (1.918−1.921 Å), consistent with the absence of intermolecular interactions.[59] The mean C−C and C−O bond lengths (1.399 Å vs 1.395 Å) and internal bond angles (86.5−180°, mean deviation ≈ 1.7°) exhibit near-perfect linear correlations with the experimental data, with R^2 = 0.9996 for bond lengths and R^2 = 0.9995 for bond angles.[60] These strong correlations are further illustrated in the regression

Table 7. Optimized Bond Lengths and Bond Angles for [Co(bzac)$_2$] Complex Calculated by DFT in Comparison with SC-XRD data

bond length	EXP (Å)	*B3LYP* (Å)	bond length	EXP (Å)	*B3LYP* (Å)
Co1—O1^i	1.9178 (9)	1.7897	C2—C3	1.3981 (15)	1.4056
Co1—O1	1.9178 (9)	1.7897	C2—C7	1.3990 (15)	1.4049
Co1—O2	1.9209 (8)	1.796	C7—C6	1.3921 (16)	1.3934
Co1—O2^i	1.9209 (8)	1.796	C5—C4	1.3903 (18)	1.3976
O1—C1	1.2770 (13)	1.311	C5—C6	1.3922 (17)	1.3976
O2—C9	1.2739 (13)	1.3114	C3—C4	1.3930 (16)	1.3916
C1—C8	1.4082 (14)	1.4004	C9—C8	1.4053 (14)	1.391
C1—C2	1.4932 (14)	1.483	C9—C10	1.5071 (15)	1.5102
bond angles	**exp (∘)**	*B3LYP* (∘)	**bond angles**	**exp (∘)**	*B3LYP* (∘)
O1^i—Co1—O1	180.0	180	C3—C2—C1	118.77 (9)	117.9136
O1^i—Co1—O2	93.48 (4)	94.1613	C7—C2—C1	122.30 (9)	123.2889
O1—Co1—O2	86.52 (4)	94.1613	C6—C7—C2	120.85 (10)	120.4628
O1^i—Co1—O2^i	86.52 (4)	85.8387	C4—C5—C6	119.93 (11)	119.6751
O1—Co1—O2^i	93.48 (4)	94.1613	C4—C3—C2	120.27 (10)	120.6445
O2—Co1—O2^i	180.0	180	C7—C6—C5	119.74 (11)	120.2658
C1—O1—Co1	126.68 (7)	129.6572	C5—C4—C3	120.33 (11)	120.1544
C9—O2—Co1	125.40 (7)	127.9538	O2—C9—C8	125.74 (9)	124.1837
O1—C1—C8	124.27 (9)	122.3517	O2—C9—C10	115.44 (9)	115.3839
O1—C1—C2	115.60 (9)	115.4125	C8—C9—C10	118.82 (9)	120.4324
C8—C1—C2	120.13 (9)	122.2358	C9 —C8—C1	123.88 (9)	121.6924
C3—C2—C7	118.89 (9)	118.7974			

plots (Figure 9a−d), where the fitted equations yield $\gamma \approx 1.002$ and $R^2 \approx 0.999$ for both bond lengths and bond angles, confirming the remarkable consistency between the experimental and DFT-optimized structures. The superimposed experimental and optimized geometries (Figure 9e) further highlight this agreement, showing an almost perfect overlap of the molecular frameworks and confirming the structural fidelity of the DFT model.

3.9.1. Frontier Molecular Orbitals (FMOs). DFT (B3LYP/LanL2DZ) calculations reveal that [Co(bzac)$_2$] possesses ligand-dominated frontier orbitals with energies of HOMO = − 5.80 eV, SOMO = − 5.73 eV, and LUMO = − 1.69 eV, leading to an overall HOMO−LUMO gap of $\Delta E \approx 4.11$ eV (Figure 10).[34] The HOMO is entirely π-type and localized on the conjugated β-diketone skeleton, while the LUMO corresponds to a π^* orbital delocalized over the phenyl rings and carbonyl groups. The SOMO represents a mixed σ(Co−O)/π state with minor but essential metal participation, fully

https://doi.org/10.1021/acs.inorgchem.5c05597
Inorg. Chem. 2026, 65, 3084−3101

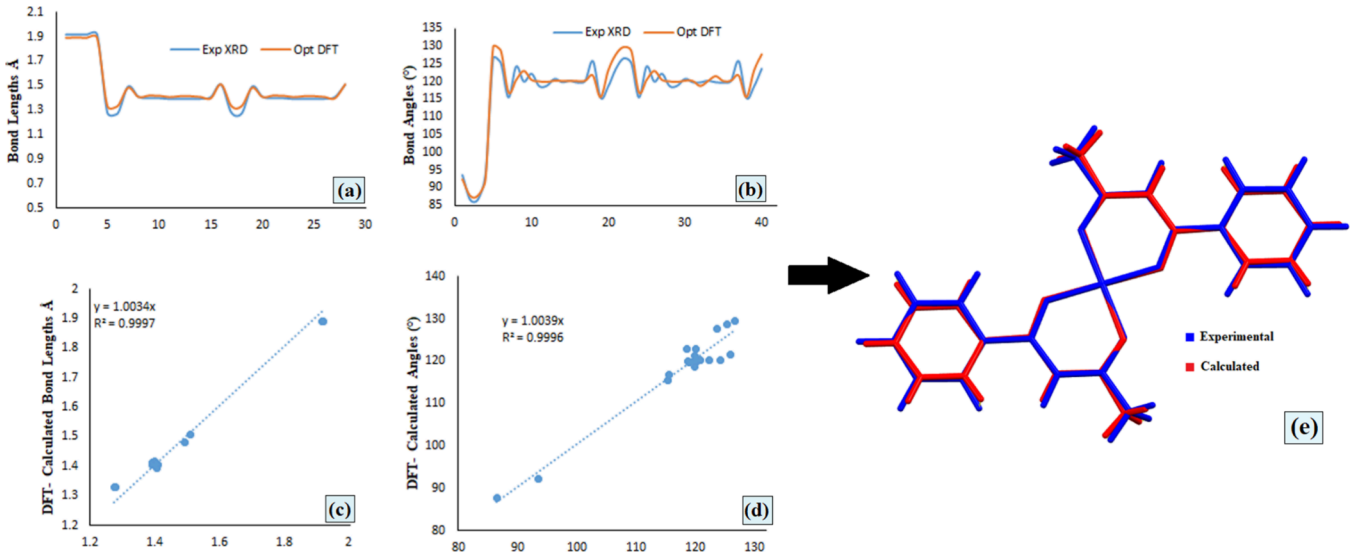

Figure 9. Comparison between experimental (SC-XRD) and DFT-optimized geometrical parameters for $[Co(bzac)_2]$: (a) bond lengths, (b) bond angles, (c–d) regression plots showing near-unity correlation ($\gamma \approx 1.003$, $R^2 > 0.999$), and (e) superposition of experimental (blue) and calculated (red) molecular structures illustrating their excellent geometrical agreement.

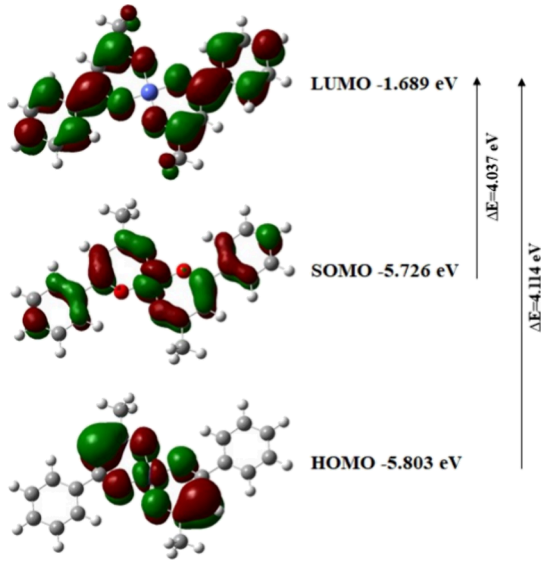

Figure 10. Frontier molecular orbitals (HOMO, SOMO, and LUMO) of $[Co(bzac)_2]$ complex with their corresponding energies and energy gaps, showing the electronic distribution and transitions within the complex.

consistent with the Co(II) d^7 electronic configuration in a quasi-square-planar coordination environment imposed by inversion symmetry. This electronic partitioning accounts for the ligand-centered $\pi \rightarrow \pi^*$ and $n \rightarrow \pi^*$ absorptions observed in the UV region, the very weak d–d tail detected around 480–500 nm, and the ν(Co–O) stretching mode appearing at 520–530 cm^{-1}, which reflects partial population of antibonding Co–O character.[35,61] The dominance of ligand-based π and π^* densities across both HOMO and LUMO rationalizes the experimentally observed π–π stacking, C–H···π, and n(O)$\rightarrow\pi$ interactions that stabilize zigzag layers parallel to (b,c) and direct the anisotropic crystal growth along [001], in full agreement with BFDH morphology predictions. The Kohn–Sham frontier spacing and the narrow HOMO–SOMO separation further support a square-planar, ligand-controlled electronic manifold in $[Co(bzac)_2]$. Without invoking cross-system numerics, this places cobalt on the planar, highly directional end of the $[M(bzac)_2]$ series, whereas p-block analogues with stereochemically active lone pairs typically exhibit reduced electronic coherence due to hemidirected distortions. This qualitative placement is fully consistent with SC-XRD/CSD comparisons and with the experimentally observed π-stacking–driven growth anisotropy.

3.9.2. Electrostatic Profile: MEP and Mulliken Charges.

The molecular electrostatic potential (MEP) surface of $[Co(bzac)_2]$ ($\pm 5.60 \times 10^{-2}$ a.u.) (Figure 11a) exhibits highly negative regions (red) centered on the chelating O atoms and the O–C = C–C = O belts, while positive potential zones (blue–cyan) occupy the aromatic periphery and methylene hydrogens.[62] This pattern reflects a ligand-polarized charge distribution, quantitatively supported by Mulliken analysis (Figure 11b and Table S1) showing Co = +0.88 au, O1 = −0.64 au, O2 = −0.61 au, and alternating positive and negative charges along the conjugated chain (C1/C2 ≈ +0.42/−0.05 au; aromatic carbons ≈ −0.17 to −0.20 au). The resulting electrostatic contrast drives short O···C intermolecular contacts (3.14–3.26 Å) between adjacent $[Co(bzac)_2]$ units, corresponding to lone-pair–π interactions where the oxygen lone pairs are attracted to the electron-poor aromatic π-systems of neighboring molecules. This perfectly matches the FMO topology, in which both HOMO and LUMO are ligand-centered (π/π^*), while the SOMO—though metal–ligand mixed—remains largely confined to the Co–O framework. Consequently, the electronic and electrostatic anisotropy imposed by this polarized π-environment governs the layered packing parallel to (b,c) and the directional growth along [001], in full agreement with BFDH morphology predictions.[63] Altogether, the MEP and Mulliken analyses confirm a highly polar Co–O core embedded in a π-delocalized ligand envelope, establishing a consistent link between electronic structure, supramolecular recognition, and macroscopic anisotropy in $[Co(bzac)_2]$. The noncovalent (n(O)$\rightarrow\pi$) contacts evidenced by the MEP correlate with low-density green regions in the RDG isosurface (Figure S1), typical of weak van der Waals

https://doi.org/10.1021/acs.inorgchem.5c05597
Inorg. Chem. 2026, 65, 3084–3101

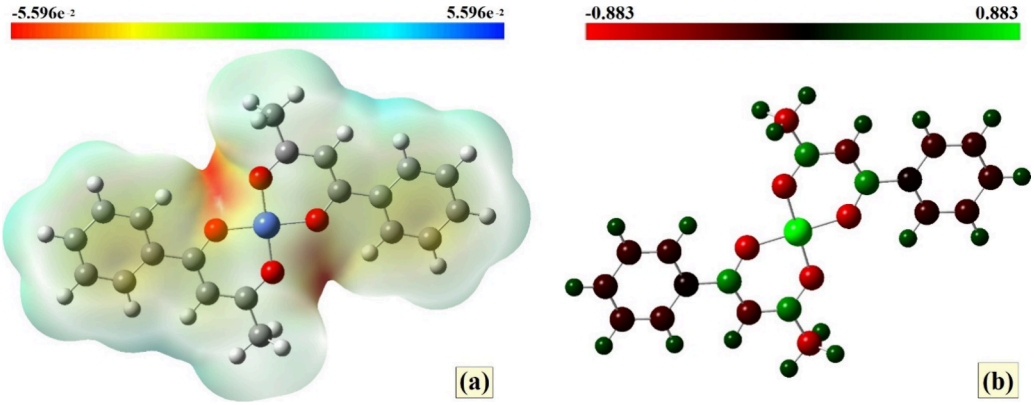

Figure 11. (a) Molecular electrostatic potential (MEP) surface of the [Co(bzac)$_2$] complex showing the spatial distribution of electrostatic potential mapped onto the electron density surface; (b) Mulliken atomic charge distribution illustrating the localized positive and negative charge regions within the molecular framework.

interactions, thus consolidating their purely noncovalent character and their role in stabilizing the crystal packing.

3.9.3. TD-DFT Electronic Excitation Analysis. To further substantiate the experimental UV−Vis assignments and to validate the electronic structure derived from crystallography and FMO analysis, TD-DFT calculations were carried out on the experimentally determined geometry of [Co(bzac)$_2$] (see Table S2). The computations predict an intense ligand-centered $\pi\rightarrow\pi$ excitation in the 2.20−2.30 eV range (≈540−565 nm), in excellent quantitative agreement with the dominant absorption band observed experimentally. A second manifold of lower-intensity transitions appears between ca. 2.00 and 2.10 eV (≈590−620 nm), arising from n→π* promotions involving oxygen lone pairs and the β-diketonate π* system; this matches the experimental shoulder extending over 600−630 nm and confirms its intraligand origin.

Importantly, all metal-centered d−d excitations are calculated at substantially lower energy and exhibit oscillator strengths close to zero ($f \ll 10^{-3}$), fully consistent with the very weak, broad tail reaching the near-infrared to deep-red region (≈800−4500 nm). This behavior is characteristic of Laporte-forbidden Co(II) d−d transitions in a near-square-planar (D_4h-like) ligand field, and aligns with the crystallographic metric revealing a highly planar CoO_4 chromophore. Altogether, the TD-DFT excitation pattern corroborates the experimental spectrum and firmly supports a model in which the low-energy optical response is metal-suppressed, while the visible region is dominated by ligand-centered π-driven activity—a structure−property relationship fully consistent with the planarity, conjugation, and electronic distribution established for [Co(bzac)$_2$].

3.10. Magnetic Context and Ligand-Field Significance of the Planar CoO_4 Core in [Co(bzac)$_2$]

Although direct magnetic measurements are not included in this study, the structural, electronic, and supramolecular attributes of [Co(bzac)$_2$] compellingly position the complex within the rapidly expanding field of four-coordinate Co(II) single-ion magnets (SIMs). Recent milestones in Co(II) magneto-chemistry have demonstrated that subtle geometric distortions, ligand-field rigidity, and donor-atom identity are decisive factors governing zero-field splitting (ZFS), magnetic anisotropy, and relaxation dynamics in low-coordinate Co(II) systems.[65−69] The crystallographically confirmed geometry of [Co(bzac)$_2$]—a strictly planar CoO_4 coordination core enforced by an inversion center and by two rigid, conjugated β-diketonate ligands—places this complex in a structurally privileged regime where pronounced single-ion anisotropy is theoretically expected, even in the absence of experimental χ(T) or AC susceptibility data.

The work of Gupta et al. established that dihedral angle control between chelating ligands is one of the most powerful geometric levers for tuning magnetic anisotropy in four-coordinate Co(II) complexes.[64] Their combined experimental and ab initio ligand-field analyses revealed that even modest variations (≈5−10°) in interchelate twisting can radically alter the orientation and magnitude of the magnetic anisotropy tensor. In this light, the nearly coplanar β-diketonate rings in [Co(bzac)$_2$]—anchored by crystallographic centrosymmetry—constitute an electronically coherent scaffold that should promote an anisotropy regime distinct from that observed in nonplanar N,N-chelated systems.

A complementary perspective is offered by Cui et al., who demonstrated that strictly oxygen-donor [CoO_4] cores can support large axial anisotropy and slow relaxation of magnetization when the ligand field is sufficiently rigid and geometrically well-defined.[65] Their results highlight that the planarity, bite angle, and π-rigidity of the chelating O-donor ligands jointly determine the splitting of the Kramers doublets and the effective relaxation barriers. Viewed in this context, the O,O′-chelation in [Co(bzac)$_2$]—with its short and nearly identical Co−O distances and planar CoO_4 coordination—matches precisely the structural criteria shown to enhance single-ion anisotropy in state-of-the-art Co(II) SIMs.

The relevance of O-donor ligands is further reinforced by Lococciolo et al., who reported slow magnetization relaxation in zero field for Co(II) complexes supported exclusively by oxygen-donor metalloligands.[66] Their results show that strong σ-donation and π-conjugation at O-donor sites can stabilize orbital-degenerate d-manifolds, thereby amplifying spin−orbit coupling and the axial ZFS parameter D. Such ligand-induced rigidity is a defining hallmark of β-diketonate coordination chemistry, and in [Co(bzac)$_2$], it is manifested through the excellent agreement between SC-XRD and DFT geometries, confirming minimal out-of-plane distortions at the metal center.

The broader theoretical framework for these observations is provided by recent Coordination Chemistry Reviews, which have systematically established the primacy of coordination number in governing anisotropy trends across Co(II) complexes. Sahu et al. highlight that four-coordinate Co(II) ions consistently exhibit the largest magnetic anisotropies

https://doi.org/10.1021/acs.inorgchem.5c05597
Inorg. Chem. 2026, 65, 3084−3101

among first-row transition metals because the reduced coordination number preserves orbital degeneracy otherwise quenched in five- or six-coordinate environments.[67] Similarly, Sarkar et al. demonstrated through computational and comparative analyses that square-planar or pseudoplanar Co(II) geometries generate the most favorable symmetry conditions for stabilizing large ZFS.[68] Against this theoretical backdrop, the square-planar CoO_4 core in $[Co(bzac)_2]$ emerges not as a structural curiosity, but rather as an electronically privileged configuration situated precisely within the parameter space identified as optimal for high anisotropy.

Together, these considerations indicate that $[Co(bzac)_2]$ represents a magnetically promising, geometrically well-defined CoO_4 platform, whose planar ligand-field environment, rigid β-diketonate backbone, and coherent supramolecular packing are all aligned with contemporary design principles for Co(II) SIMs. While the confirmation of slow magnetic relaxation requires future AC susceptibility measurements on larger sample quantities, the present SC-XRD and DFT analyses firmly position this complex within the landscape of structurally encoded anisotropic Co(II) systems. In this sense, $[Co(bzac)_2]$ stands as a valuable, CSD-anchored benchmark that links planarity-enforced ligand-field symmetry, oxygen-donor covalency, and single-ion magnetic potential, offering a structurally pristine reference point for future experimental and computational magnetic investigations.

4. CONCLUSION

This study positions $[Co(bzac)_2]$ as a structurally definitive member of the $[M(bzac)_2]$ series (M = Pb, Sn, P$\hat{d}$trans, P$\hat{d}$cis, Cu), offering a unified framework for understanding how coordination symmetry and chelate planarity direct supramolecular organization and crystal morphology. The combination of quantitative planarity metrics, targeted CSD analysis, and BFDH morphology modeling reveals a continuous structural evolution across the series: moving from stereochemically active p-block centers to square-planar d-block ions systematically enhances chelate coplanarity and strengthens $\pi-\pi$, metal$-\pi$, C$-$H$\cdots\pi$, and O$\cdots$C(lp$\rightarrow\pi$) interactions. Within this progression, $[Co(bzac)_2]$ lies at the most planar and cohesively stacked limit, where densely aligned aromatic columns and short noncovalent contacts generate a pronounced growth anisotropy fully consistent with the experimentally observed acicular habit and with the PXRD signature of the dominant (002) stacking plane.

Spectroscopic and theoretical results converge on a ligand-dominated electronic structure, in which the CoO_4 chromophore governs the geometric constraint while the conjugated β-diketonate system shapes the optical response. The strong agreement between SC-XRD and DFT geometries, the MEP-supported assignment of noncovalent contacts, and the accurate TD-DFT reproduction of the UV$-$Vis envelope collectively validate a coherent structure$-$electronics$-$optics relationship. The rigid, centrosymmetric tetracoordinate environment further situates $[Co(bzac)_2]$ within the design space of low-coordinate Co(II) systems of growing interest for their potential magnetic anisotropy.

Taken together, these results provide a transferable blueprint for interpreting and predicting morphology in planar O-donor complexes. By integrating comparative crystallography, supramolecular interaction mapping, BFDH morphology prediction, and electronic-structure calculations within a unified SC-XRD $\leftrightarrow$ CSD $\leftrightarrow$ BFDH $\leftrightarrow$ DFT workflow, this work establishes the $[M(bzac)_2]$ family as a reference platform for quantitatively linking molecular planarity, packing directionality, and macroscopic anisotropy. Beyond the specific case of cobalt, the methodological framework and validated structure$-$morphology descriptors developed here offer the broader community a robust and adaptable toolset for the rational design of anisotropic coordination materials with targeted optical or magnetic functionalities.

■ ASSOCIATED CONTENT

Supporting Information

The Supporting Information is available free of charge at https://pubs.acs.org/doi/10.1021/acs.inorgchem.5c05597.

Mulliken atomic charges for the $[Co(bzac)_2]$ complex (Table S1); reduced density gradient (RDG) isosurface analysis highlighting noncovalent interactions (Figure S1); TD-DFT calculated vertical excitation energies, dominant orbital contributions, and electronic assignments for $[Co(bzac)_2]$ (Table S2) (PDF)

Accession Codes

Deposition Number 2498791 contains the supplementary crystallographic data for this paper. These data can be obtained free of charge via the joint Cambridge Crystallographic Data Centre (CCDC) and Fachinformationszentrum Karlsruhe Access Structures service.

■ AUTHOR INFORMATION

Corresponding Author

Rim Benali-Cherif − *Laboratoire des Structures, Propriétés et Interactions Interatomiques (LASPI2A), Université Abbes Laghrour-Khenchela, Khenchela 40000, Algeria;* orcid.org/0000-0002-6873-8840; Email: benalicherif.rim@univ-khenchela.dz

Authors

Oumaima Ghodbane − *Laboratoire des Structures, Propriétés et Interactions Interatomiques (LASPI2A), Université Abbes Laghrour-Khenchela, Khenchela 40000, Algeria*

Radhwane Takouachet − *Laboratoire des Structures, Propriétés et Interactions Interatomiques (LASPI2A), Université Abbes Laghrour-Khenchela, Khenchela 40000, Algeria*

Wahiba Falek − *Laboratoire des Structures, Propriétés et Interactions Interatomiques (LASPI2A), Université Abbes Laghrour-Khenchela, Khenchela 40000, Algeria*

Alessia Bacchi − *Dipartimento di Scienze Chimiche, della Vita e della Sostenibilità Ambientale, Università di Parma, Parma 43124, Italy; Biopharmanet-Tec, Università di Parma, Parma 43124, Italy;* orcid.org/0000-0001-5675-9372

Andrea Daolio − *Dipartimento di Scienze Chimiche, della Vita e della Sostenibilità Ambientale, Università di Parma, Parma 43124, Italy;* orcid.org/0000-0003-3571-3935

El-Eulmi Bendeif − *Synchrotron SOLEIL, Saint-Aubin 91190, France; Université de Lorraine, CNRS, CRM2, Nancy F-54000, France*

Nourredine Benali-Cherif − *Académie Algérienne des Sciences et de la Technologie (AAST), Algiers 16028, Algeria; University of JIJEL, Jijel 18000, Algeria*

Complete contact information is available at: https://pubs.acs.org/10.1021/acs.inorgchem.5c05597

https://doi.org/10.1021/acs.inorgchem.5c05597
Inorg. Chem. 2026, 65, 3084−3101

Notes

The authors declare no competing financial interest.

■ ACKNOWLEDGMENTS

We gratefully acknowledge Professor Abdelkader Djelloul for performing the UV−Vis measurements and Professor Abdecharif Boumaza for conducting the IR spectroscopy experiments. We also thank the X-ray diffraction platform PMD^{2}X of the Université de Lorraine for providing access to single-crystal X-ray diffraction facilities, and the Department of Chemistry, Life Sciences and Environmental Sustainability, University of Parma (Italy), for performing the powder X-ray diffraction measurements. Financial support from the Algerian MESRS (Ministère de l'Enseignement Supérieur et de la Recherche Scientifique), the DGRSDT (Direction Générale de la Recherche Scientifique et du Développement Technologique), and Abbes Laghrour Khenchela University is warmly acknowledged.

■ REFERENCES

(1) Son, Y. J.; Kim, D.; Park, J. W.; Yu, Y.; Hwang, S. J. Coordination Chemistry of Ligands Bearing Heavy Group 14 and 15 Elements: Comparative Analysis of Their Influence on Transition Metal Chemistry. *Coord. Chem. Rev.* **2025**, *526*, No. 216317.

(2) Lewandowski, E. C.; Arban, C. B.; Deal, M. P.; Batchev, A. L.; Allen, M. J. Europium(II/III) Coordination Chemistry toward Applications. *Chem. Commun.* **2024**, *60*, 10655−10671.

(3) Castro-Ramírez, R.; Barba-Behrens, N. A New Therapeutic Perspective on Metal-Based Drugs. *Dalton Trans.* **2025**, 15964.

(4) Kainat, S. F.; Hawsawi, M. B.; Mughal, E. U.; Naeem, N.; Almohyawi, A. M.; Altass, H. M.; Hussein, E. M.; Sadiq, A.; Moussa, Z.; Abd-El-Aziz, A. S.; Ahmed, S. A. Recent Developments in the Synthesis and Applications of Terpyridine-Based Metal Complexes: A Systematic Review. *RSC Adv.* **2024**, *14* (30), 21464−21537.

(5) Lee, L. C.; Lo, K. K.-W. Luminescent Transition Metal Complexes for Bioimaging and Sensing. *Chem. Rev.* **2024**, *124* (15), 8825−9014.

(6) Gutmańska, K.; Podborska, A.; Mazur, T.; Sławek, A.; Sivasamy, R.; Maximenko, A.; Orzeł, Ł.; Oszajca, J.; Stochel, G.; Dev, A. V.; Vijayakumar, C.; Szaciłowski, K.; Dołęga, A. From Donor-Acceptor Ligands to Smart Coordination Polymers: Cyanothiazole-Cu(I) Complexes for Multifunctional Electronic Devices. *Chem. - Eur. J.* **2025**, *31* (31), No. e202500215.

(7) Sabeg, Y.; Benali-Cherif, R.; Falek, W.; Takouachet, R.; Golea, L.; Aygün, M.; Benali-Cherif, N. Comprehensive Study of a Novel Cobalt(II) Complex: Synthesis, X-Ray Crystal Structure, Hirshfeld Surface Analysis, Computational Quantum Investigations, and Molecular Docking Insights. *Polyhedron* **2025**, *271*, No. 117445.

(8) Tubau, À.; Rodríguez, L.; Pander, P.; Weatherill, L.; Dias, F. B.; Font-Bardía, M.; Vicente, R. Slow magnetic relaxation and luminescence properties in β-diketonate lanthanide(III) complexes. Preparation of Eu(III) and Yb(III) OLED devices. *J. Mater. Chem. C* **2024**, *12* (22), 8127−8144.

(9) Zhang, W.; Wei, S.; Zhang, G.; Yang, J.; Peng, L.; Zhang, S. The Roles of β-Diketones and Their Derivatives in the Design of Photocatalysts. *Coord. Chem. Rev.* **2025**, *524*, No. 216318.

(10) Tubau, À.; Gómez-Coca, S.; Speed, S.; Font-Bardía, M.; Vicente, R. New Series of Mononuclear β-Diketonate Cerium(III) Field-Induced Single-Molecule Magnets. *Dalton Trans.* **2024**, *53*, 9387−9405.

(11) Mahesha; Udaya Kumar, A. H.; Pampa, K. J.; Lokanath, N. K. The Investigation of Modification in Structural Flexibility and Coordination Modes in a Solvent-Free β-Diketone Cu(II) Complex by Crystal Structure and DFT Studies. *Polyhedron.* **2023**, *238*, No. 116293.

(12) Saraiva, L. F.; Beltrame, A. C. F.; Bispo-Jr, A. G.; Canisares, F. S. M.; Carneiro Neto, A. N.; Moura, R. T., Jr; Kraka, E.; Lima, S. A. M.; Pires, A. M. Unfolding the Photophysical Behavior of Luminescent Polymeric Films Containing β-Diketonate Tetrakis Eu(III) Complexes via Multilayer Quantum Mechanics. *ACS Omega.* **2025**, *10* (28), 30563−30575.

(13) Üngör, Ö.; Sanchez, S.; Ozvat, T. M.; Zadrozny, J. M. Asymmetry-Enhanced ^59Co NMR Thermometry in Co(III) Complexes. *Inorg. Chem. Front.* **2023**, *10*, 7064−7072.

(14) Barszcz, B.; Masternak, J.; Kowalik, M. Structural Insights into Coordination Polymers Based on 6s^2 Pb(II) and Bi(III) Centres Connected via Heteroaromatic Carboxylate Linkers and Their Potential Applications. *Coord. Chem. Rev.* **2021**, *443*, No. 213935.

(15) Harriswangler, C.; Freire-García, A.; Argibay-Otero, S.; Rodríguez-Rodríguez, A.; Rodríguez, J. M.; Esteban-Gómez, D.; Vázquez-López, E. M.; Platas-Iglesias, C. Structural Effects of the Pb^{2+} 6s^2 Lone Pair Activity: Eccentricity. *Coord. Chem. Rev.* **2025**, *529*, No. 216434.

(16) Maverick, A. W. Structural Flexibility of Metal Chelate Complexes and Its Relation to Supramolecular Chemistry. *Helv. Chim. Acta* **2023**, *106*, No. e202200160.

(17) Martynova, S.; Krisyuk, V.; Sukhikh, A.; Benassi, E. β-Diketonate Coordination: Vibrational Properties, Electronic Structure, Molecular Topology, and Intramolecular Interactions. Beryllium(II), Copper(II), and Lead(II) as Study Cases. *J. Phys. Chem. A* **2025**, *129* (4), 924−945.

(18) Mirtamizdoust, B.; Karamad, A.; Mojtabazade, F.; Hosein-Monfared, H.; Bikas, R.; Zák, Z.; Erfani, H.; Jadoun, S.; Mishra, A. K. Exploring C−F···π Interactions: Synthesis, Characterization, and Surface Analysis of Copper β-Diketone Complexes. *ACS Omega* **2024**, *9* (5), 5563−5575.

(19) Stienen, C.; Grahl, J.; Wölper, C.; Schulz, S.; Bendt, G. Fluorinated β-Diketonate Complexes M(tfac)$_2$(TMEDA) (M = Fe, Ni, Cu, Zn) as Precursors for the MOCVD Growth of Metal and Metal Oxide Thin Films. *RSC Adv.* **2022**, *12* (35), 22974−22983.

(20) Buitendach, B. E.; Erasmus, E.; Conradie, J.; Niemantsverdriet, J. W.; Lang, H.; Swarts, J. C. Synthesis, Electrochemistry, XPS, and DFT Calculations of α-Carbon-Bonded Gold(I) Ferrocenyl- and Ruthenocenyl-Containing β-Diketonato Complexes. *Organometallics* **2024**, *43* (12), 1334−1348.

(21) Aouachria, C.; Benali-Cherif, R.; Takouachet, R.; Missaoui, D.; Rahmouni, A.; Aggoun, K.; Kaaboub, L.; Benali-Cherif, N.; Gouasmia, A. Theoretical and Experimental Study of Novel Vanillin-Derivatives: Structural Characterization, Unconventional Vanillin Reactivity, and Biological Applications. *J. Mol. Struct.* **2025**, *1442*, No. 142709.

(22) Zhang, C.; Wang, Z.; Si, W. D.; Chu, H.; Zhou, L.; Li, T.; Huang, X. Q.; Gao, Z. Y.; Azam, M.; Tung, C. H.; Cui, P.; Sun, D. Dynamic and Transformable Cu_{12} Cluster-Based C−H···π-Stacked Porous Supramolecular Frameworks. *Nat. Commun.* **2023**, *14*, 6413.

(23) Nakajima, K.; Ozaki, M. Anisotropic Crystal Growth in Blue Phase I Transitioned from a Uniformly Oriented Cholesteric Phase. *Soft Matter* **2024**, *20*, 4072−4078.

(24) Bedghiou, D.; Rahab, M. N.; Benali-Cherif, R.; Djelloul, A.; Boumaza, A. First-Principles Unveiling Equilibrium Shapes for Understanding Morphological Growth Mechanisms in Alumina Polymorphs. *Acta Mater.* **2024**, *281*, No. 120450.

(25) Messalaoui, H.; Takouachet, R.; Benali-Cherif, R.; Falek, W.; Golea, L.; Marir, A.; Jeanneau, E.; Ghodbane, O.; Benali-Cherif, N. Bio-Inspired One-Dimensional Cadmium Halide Stabilized by Cytosinium: Structural, Spectroscopic and Theoretical Investigations. *J. Mol. Struct.* **2026**, *1351*, No. 144216.

(26) Sheldrick, G. M. A Short History of SHELX. *Acta Cryst. A* **2008**, *64* (1), 112−122.

(27) Sheldrick, G. M. Crystal Structure Refinement with SHELXL. *Acta Crystallogr. Sect. C Struct. Chem.* **2015**, *71* (Pt 1), 3−8.

(28) Krause, L.; Herbst-Irmer, R.; Sheldrick, G. M.; Stalke, D. Comparison of Silver and Molybdenum Microfocus X-Ray Sources for Single-Crystal Structure Determination. *J. Appl. Crystallogr.* **2015**, *48*, 3−10.

(29) Macrae, C. F.; Sovago, I.; Cottrell, S. J.; Galek, P. T. A.; McCabe, P.; Pidcock, E.; Platings, M.; Shields, G. P.; Stevens, J. S.; Towler, M.; Wood, P. A. Mercury 4.0: From Visualization to Analysis, Design and Prediction. *J. Appl. Crystallogr.* **2020**, *53*, 226−235.

https://doi.org/10.1021/acs.inorgchem.5c05597
Inorg. Chem. 2026, 65, 3084−3101

(30) Ziegler, T. Approximate Density Functional Theory as a Practical Tool in Molecular Energetics and Dynamics. *Chem. Rev.* **1991**, *91*, 651−667.
(31) Trucks, G. W.; Frisch, M. J.; Scuseria, G. E.; Schlegel, H. B.; Robb, M. A.; Cheeseman, J. R.; Scalmani, G.; Barone, V.; Mennucci, B.; Petersson, G. A.; Nakatsuji, H.; Caricato, M.; Li, X.; Hratchian, H. P.; Izmaylov, A. F.; Bloino, J.; Zheng, G.; Sonnenberg, J. L.. *Gaussian 09*; Gaussian, Inc.: Wallingford, CT, 2009.
(32) Dennington, R.; Keith, T. A.; Millam, J. M.. *GaussView, Version 6*; Semichem Inc.: Shawnee Mission, KS, 2016.
(33) Joksimović, N.; Petronijević, J.; Ćoćić, D.; Ristić, M.; Mihajlović, K.; Janković, N.; Milović, E.; Klisurić, O.; Petrović, N.; Kosanić, M. Synthesis, Characterization, and Biological Evaluation of Novel Cobalt(II) Complexes with β-Diketonates: Crystal Structure Determination, BSA Binding Properties and Molecular Docking Study. *J. Biol. Inorg. Chem.* **2024**, *29* (5), 541−553.
(34) Dorovskikh, S. I.; Sukhikh, A. S.; Yatygin, V. A.; Turgambaeva, A. E.; Maximovskiy, E. A.; Pishchur, D. P.; Vikulova, E. S. Cobalt(II) Complexes with Fluorinated β-Diketones and Their Derivatives for MOCVD Applications. *Russ. J. Gen. Chem.* **2025**, *95* (3), 690−703.
(35) Conradie, M. M. Cu(β-diketonato)2_22 Bathochromic Shifts from the Ultraviolet towards the Visible Region. *J. Mol. Model.* **2024**, *30*, 336.
(36) Ewings, P. F. R.; Harrison, P. G.; King, T. J. Crystal and Molecular Structure of Bis(1-phenylbutane-1,3-dionato)Tin(II). *J. Chem. Soc., Dalton Trans.* **1975**, 1455−1458.
(37) Deng, J. H.; Luo, J.; Mao, Y. L.; Lai, S.; Gong, Y. N.; Zhong, D. C.; Lu, T. B. π-π Stacking Interactions: Non-negligible Forces for Stabilizing Porous Supramolecular Frameworks. *Sci. Adv.* **2020**, *6* (2), No. eaax9976.
(38) Takouachet, R.; Benali-Cherif, R.; Bendeif, E. E.; Bouchouit, K.; Falek, W.; Sahraoui, B.; Rahmouni, A.; Benali-Cherif, N. Nonlinear Optical Properties and Structural Characterization of a Series of Carboxyanilinium Hydrogen Selenite Hybrids: Synthesis, First-Principles Calculations and Correlation Analysis for Advanced Photonic Applications. *Inorg. Chem. Commun.* **2024**, *170*, No. 113439.
(39) Kurpik, G.; Wachowicz, W.; Walczak, A.; Harrowfield, J.; Stefankiewicz, A. R. Pyridyl-β-diketonates: Versatile Ligands for Generation of Functional Nanostructures. *Coord. Chem. Rev.* **2025**, *539*, No. 216762.
(40) Mangundu, P.; Ho, C. C.; Fuller, R. O. Recent Developments in Magnetic Lanthanoid Complexes Supported by β-Diketonate or Pyridyl-Pyrazolate Ligands. *Inorg. Chim. Acta* **2026**, *535*, No. 122878.
(41) Ghouari, N.; Benali-Cherif, R.; Takouachet, R.; Falek, W.; Missaoui, D.; Rahmouni, A.; Bendeif, E.-E.; Benali-Cherif, N. Crystal Engineering of a New Pharmaceutical Polymorph of Gallic Acid Monohydrate: A Structural Comparative Study and Chemical Computational Quantum Investigations. *CrystEngComm* **2023**, *25*, 6279−6290.
(42) Benali-Cherif, R.; Takouachet, R.; Falek, W.; Benali-Cherif, N.; Jelsch, C.; Merazig, H.; Hafied, M.; Bendeif, E.-E.; Mokhnachi, N. B.; Taibi, K. Synthesis, Structural Elucidation, Spectroscopic, Hirshfeld Surface Analysis and Theoretical Simulation of a New Adeninium Orthoperiodate(1−) Bis(hydrate) Organic−Inorganic Hybrid Crystals. *J. Mol. Struct.* **2021**, *1224*, No. 129034.
(43) Derardja, A.-A.; Golea, L.; Benali-Cherif, R.; Luneau, D.; Boutobba, Z.; Boumedjane, Y.; Harkat, H. Synthesis, Crystal Structure, DFT Calculations, Hirshfeld Surface Analysis and Molecular Docking Studies of a New Manganese Complex. *Inorg. Chem. Commun.* **2022**, *146*, No. 110198.
(44) Pramanik, S.; Pathak, S.; Frontera, A.; Mukhopadhyay, S. Exploration of Supramolecular and Theoretical Aspects of Two New Cu(II) Complexes: On the Importance of Lone-Pair$\cdots\pi$(Chelate Ring) and $\pi\cdots\pi$(Chelate Ring) Interactions. *J. Mol. Struct.* **2022**, *1265*, No. 133358.
(45) Jana, S.; Khan, S.; Bauzá, A.; Frontera, A.; Chattopadhyay, S. The Crucial Role of Chelate−Chelate Stacking Interactions in the Crystal Structure of a Square-Planar Cu(II) Complex. *J. Mol. Struct.* **2017**, *1127*, 355−360.
(46) Takouachet, R.; Benali-Cherif, R.; Bendeif, E. E.; Jelsch, C.; Cherif, F. Y.; Rahmouni, A.; Benali-Cherif, N. The Supramolecular Behavior and Molecular Recognition of Adeninium Cations on Anionic Hydrogen Selenite/Diselenite Frameworks: A Structural and Theoretical Analysis. *J. Mol. Struct.* **2021**, *1229*, No. 129836.
(47) Groom, C. R.; Bruno, I. J.; Lightfoot, M. P.; Ward, S. C. The Cambridge Structural Database. *Acta Crystallogr., Sect. B: Struct. Sci., Cryst. Eng. Mater.* **2016**, *72*, 171−179.
(48) Cox, E. G.; Shorter, A. J.; Wardlaw, W. "Stereochemistry of Bivalent Tin and Lead.". *Nature* **1937**, *139*, 71−72.
(49) Hon, P. K.; Pfluger, C. E.; Belford, R. L. Bis(1-phenyl-1,3-butanedionato)palladium(II). Crystal and molecular structure of the trans form. *Inorg. Chem.* **1967**, *6*, 730−735.
(50) Okeya, S.; Asai, H.; Ooi, S. I.; Matsumoto, K.; Kawaguchi, S.; Kuroya, H. cis-Bis(benzoylacetonato)palladium(II). *Inorg. Nucl. Chem. Lett.* **1976**, *12* (9), 677−680.
(51) Hon, P. K.; Pfluger, C. E.; Belford, R. L. The Molecular and Crystal Structure of Bis(1-phenyl-1,3-butanedionato)copper(II). *Inorg. Chem.* **1966**, *5* (4), 516−521.
(52) Dey, S. K.; Bag, B.; Zhou, Z.; Chan, A. S. C.; Mitra, S. Synthesis, Characterization, and Crystal Structure of a Monomeric and a Macrocyclic Copper(II) Complex with a Large Cavity Using Benzylacetylacetone Ligand. *Inorg. Chim. Acta* **2004**, *357* (7), 1991−1996.
(53) Krishnegowda, H. M.; Karthik, C. S.; Marichannegowda, M. H.; Kumara, K.; Kudigana, P. J.; Lingappa, M.; Mallu, P.; Neratur, L. K. Synthesis and Structural Studies of 1-Phenyl-1,3-butanedione Copper-(II) Complexes as Excellent Antimicrobial Agents against Methicillin-Resistant *Staphylococcus aureus*. *Inorg. Chim. Acta* **2019**, *484*, 227−236.
(54) Hadjiivanov, K. I.; Panayotov, D. A.; Mihaylov, M. Y.; Ivanova, E. Z.; Chakarova, K. K.; Andonova, S. M.; Drenchev, N. L. Power of Infrared and Raman Spectroscopies to Characterize Metal−Organic Frameworks and Investigate Their Interaction with Guest Molecules. *Chem. Rev.* **2021**, *121* (3), 1286−1424.
(55) Abd-ElRazek, S. E.; El-Gamasy, S. M. New Benzoyl Acetohydrazone-Based Metal Complexes with Viral DNA Binding and Cleavage and Antimicrobial Treatments: Synthesis and Biological Activities. *J. Mol. Struct.* **2023**, *1274*, No. 134457.
(56) Del Gobbo, J.; Santini, C.; Dolmella, A.; Li, Z.; Caviglia, M.; Pellei, M. New Copper Complexes with N,O-Donor Ligands Based on Pyrazole Moieties Supported by 3-Substituted Acetylacetone Scaffolds. *Molecules* **2024**, *29* (3), 621.
(57) Panova, E. V.; Voronina, J. K.; Safin, D. A. Methyl- versus Ethyl-Directed Formation of Square-Planar Cobalt(II) and Octahedral Cobalt(III) Chelates of the *In Situ* Generated Schiff Bases. *Polyhedron.* **2024**, *257*, No. 117014.
(58) Reyna, J. A.; Krishnan, V. M.; Silva Villatoro, R.; Arman, H. D.; Stoian, S. A.; Tonzetich, Z. J. Square-Planar Imido Complexes of Cobalt: Synthesis, Reactivity and Computational Study. *Dalton Trans.* **2024**, *53*, 12128−12137.
(59) Dhimba, G.; Müller, A.; Lammertsma, K. Racemization Pathway for $MoO_2(acac)_2$ Favored over Ray−Dutt, Bailar, and Conte−Hippler Twists. *Inorg. Chem.* **2022**, *61* (38), 14918−14923.
(60) Kupietz, K.; Gomila, R. M.; Roisnel, T.; Frontera, A.; Gramage-Doria, R. Shortening C—N$\cdots$Br—C_{sp3} Halogen Bonds via π-Stacking. *CrystEngComm* **2024**, *26* (16), 2131−2135.
(61) Tahirli, S.; Sadeghian, N.; Aliyeva, F.; Sujayev, A.; Günay, S.; Erden, Y.; Shikhaliyev, N.; Kaya, S.; Mehtap Özden, E.; Chiragov, F.; Berisha, A.; Taslimi, P. New Azo Derivative of β-Diketones and Its Cu(II), Co(II) Complexes: Synthesis, Theoretical Study and Biological Activity. *Chem. Biodivers.* **2024**, *21* (4), No. e202301861.
(62) Bera, S.; Bhunia, S.; Gomila, R. M.; Frontera, A.; Chattopadhyay, S. Synthesis, Structural Characterization, and DFT Investigation of a Mixed-Valence Co(III)/Co(II) Complex Stabilized by Supramolecular Interactions. *RSC Adv.* **2025**, *15*, 15530−15538.
(63) Ashfaq, M.; Tahir, M. N.; Muhammad, S.; Munawar, K. S.; Ali, A.; Bogdanov, G.; Alarfaji, S. S. Single-Crystal Investigation, Hirshfeld Surface Analysis, and DFT Study of Third-Order NLO Properties of

https://doi.org/10.1021/acs.inorgchem.5c05597
Inorg. Chem. 2026, 65, 3084−3101

Unsymmetrical Acyl Thiourea Derivatives. *ACS Omega* **2021**, *6* (46), 31211−31225.
(64) Gupta, S. K.; Rao, S. V.; Demeshko, S.; Dechert, S.; Bill, E.; Atanasov, M.; Neese, F.; Meyer, F. Air-Stable Four-Coordinate Cobalt(II) Single-Ion Magnets: Experimental and *Ab Initio* Ligand Field Analyses of Correlations between Dihedral Angles and Magnetic Anisotropy. *Chem. Sci.* **2023**, *14*, 6355−6374.
(65) Cui, H.-H.; Xu, H.; Zhang, T.; Chen, Q.; Luo, S.; Wang, M.; Wang, J.; Chen, L.; Zhang, M.; Tang, Y. Magnetic Anisotropy and Relaxation in Four-Coordinate Cobalt(II) Single-Ion Magnets with a [CoII O_4] Core. *Inorg. Chem.* **2024**, *63*, 9050−9057.
(66) Lococciolo, G.; Gupta, S. K.; Dechert, S.; Demeshko, S.; Duboc, C.; Atanasov, M.; Neese, F.; Meyer, F. Oxygen-Donor Metalloligands Induce Slow Magnetization Relaxation in Zero Field for a Cobalt(II) Complex with a {CoO_4} Motif. *Inorg. Chem.* **2024**, *63*, 5652−5663.
(67) Kumar Sahu, P.; Kharel, R.; Shome, S.; Goswami, S.; Konar, S. Understanding the Unceasing Evolution of Co(II)-Based Single-Ion Magnets. *Coord. Chem. Rev.* **2023**, *475*, No. 214871.
(68) Sarkar, A.; Dey, S.; Rajaraman, G. Role of Coordination Number and Geometry in Controlling the Magnetic Anisotropy in FeII, CoII, and NiII Single-Ion Magnets. *Chem. - Eur. J.* **2020**, *26*, 14036−14058.

https://doi.org/10.1021/acs.inorgchem.5c05597
Inorg. Chem. 2026, 65, 3084−3101